ABSTRACT

ALSAIARI, ABDULRAHMAN MUBARAK. Intelligent Flow Chemistry: A Data-Driven Approach to Autonomous Inorganic Synthesis. (Under the direction of Dr. Milad Abolhasani).

The accelerated discovery of advanced functional materials is essential to addressing urgent global challenges related to energy and sustainability. Although self-driving laboratories (SDLs) and materials acceleration platforms (MAPs) have made notable advances, their ability to navigate complex synthesis spaces remains constrained by limited data throughput. In this work, we present Dynamic Flow Experiments (DFEs) as a data intensification approach implemented within Self-Driving Fluidic Laboratories (SDFLs), enabling the continuous translation of transient reaction conditions into their steady-state counterparts. Using CdSe colloidal quantum dots as a model system, DFEs demonstrated a significant enhancement—exceeding an order of magnitude—in data acquisition efficiency, while also minimizing time and reagent usage compared to conventional SDFL methods. Through the integration of in-situ, real-time optical characterization, microscale flow chemistry, and autonomous control, DFEs redefine how data is leveraged in SDFLs, substantially accelerating material discovery and optimization while advancing the sustainability of autonomous research frameworks.

Intelligent Flow Chemistry: A Data-Driven Approach to Autonomous Inorganic Synthesis

by
Abdulrahman Alsaiari

A thesis submitted to the Graduate Faculty of
North Carolina State University
in partial fulfillment of the
requirements for the degree of
Master of Science

Chemical Engineering

Raleigh, North Carolina
2025

APPROVED BY:

_____	_____
Dr. Milad Abolhasani Committee Chair	Dr. Michael Dickey
_____	
Dr. Qingshan Wei	

DEDICATION

To my beloved family, whose unwavering support and encouragement have been my foundation, and to my friends and mentors who guided me with their wisdom throughout this academic journey, this work is dedicated to you with deepest gratitude.

BIOGRAPHY

Abdulrahman Alsaiari was born and raised in Saudi Arabia. He received a fully funded scholarship from the Saudi Ministry of Education to pursue higher education in the United States, where he earned his bachelor's degree in chemical engineering from Oregon State University.

Following his undergraduate studies, Abdulrahman worked as a project engineer at AES, a vendor for Saudi Aramco, where he supervised the execution of several oil and gas projects involving chemical injection systems and modular skids. He later joined Saudi Aramco and contributed to the construction of a major NGL gas plant as part of the Marjan Increment Project.

Motivated by a strong interest in research and innovation, Abdulrahman pursued a master's degree in chemical engineering at North Carolina State University. During his graduate studies, he worked under the supervision of Dr. Milad Abolhasani, focusing on the development of self-driving laboratories and the use of automation in accelerated materials discovery.

ACKNOWLEDGMENTS

First and foremost, I would like to express my deepest gratitude to my advisor, Dr. Milad Abolhasani, for his invaluable guidance, continuous support, and strong encouragement throughout the course of my graduate studies. His mentorship has been instrumental in shaping my academic and research journey.

I would also like to sincerely thank the other members of my thesis committee, Dr. Michael Dickey and Dr. Qingshan Wei, for their time, insightful feedback, and generous support. Their expertise and perspectives have greatly enriched this work.

I would like to extend a special thanks to my friend and senior Ph.D. colleague, Fernando Delgado-Licona, for his outstanding guidance and continuous support, both personally and professionally. His mentorship was essential in helping me navigate the fundamentals of machine learning and self-driving laboratory systems. His contributions to this work, and to my growth as a researcher, are deeply appreciated.

A special thanks goes to my colleagues and lab members for their collaboration, insightful discussions, and the friendship that made the research process both productive and enjoyable.

I would also like to sincerely acknowledge two very special friends, Yahya Alzahrani and Dr. Fares Alzahrani. Their constant support, encouragement, and care have meant the world to me. They were more than just friends—they were my family in the United States during a time when I was far from home. Their presence, motivation, and emotional support were a source of strength throughout this journey. Without them, this experience would have been much more difficult. I am truly grateful for their unwavering companionship and the role they played in helping me reach this milestone.

I would also like to extend my deepest gratitude to my fiancée, whose constant support and presence were a source of strength throughout this journey. Her encouragement, patience, and

unshakable belief in me helped carry me through the most challenging and stressful days. She stood by my side through every high and low, offering comfort and motivation when I needed it most. I am truly thankful for her love, sacrifices, and the emotional stability she provided during this transformative chapter of my life.

I gratefully acknowledge the Saudi Ministry of Education for granting me the scholarship that allowed me to pursue my education and research in the United States. Without this opportunity, none of this would have been possible.

Finally, I would like to express my heartfelt appreciation to my family and friends for their constant love, patience, and support throughout my academic journey. Their belief in me has been a continual source of strength and motivation.

TABLE OF CONTENTS

LIST OF TABLES

LIST OF FIGURES

Chapter 1 : INTRODUCTION

1.1 The Need for Sustainable Innovation in Chemical Engineering

Chemical engineering has been a driving force behind the industrial revolution, enabling transformative innovations ranging from the discovery and manufacture of life-saving pharmaceuticals to the large-scale production of essential goods. These advancements have profoundly enhanced the global quality of life by enabling access to critical products and services. However, the rapid expansion of chemical manufacturing has also introduced significant environmental and resource consumption challenges, including climate change, ecosystem degradation, and the depletion of finite resources.[1] This urgency is further underscored by time-sensitive energy, environment, and healthcare targets, necessitating swift and deliberate action. Meeting these challenges requires global collaboration efforts and rethinking scientific innovation. Self-driving labs (SDLs) have recently emerged as a promising tool to enhance research efficiency and speed. Yet, their development must be informed by a forward-looking approach that aligns with broader sustainability and societal goals.

SDLs offer an integrated framework for accelerating research in domains where the scale and complexity of experimental design surpass what individual researchers can feasibly manage. By automating the design–make–test–analyze (DMTA) cycle, SDLs leverage both prior knowledge and simulated experiments, dynamically refining their knowledge model in real time with minimal human supervision. Central to this workflow is an artificial intelligence (AI)-assisted decision-making system that orchestrates the entire process—analyzing incoming data, pinpointing promising experimental pathways, and iteratively updating predictive models. SDLs have demonstrated success in rapid discovery, optimization, process development, and

manufacturing of advanced materials and (bio)molecules.[2] A key aspect of the SDL operation lies in the interplay between its digital and physical components: physical modules handle (bio)chemical formulation, transport, synthesis, purification, and characterization, while digital modules automate data collection, analysis, and experimental design. This closed-loop coordination of (qu)bits and atoms significantly boosts the speed, precision, and information density of scientific research.[3] (Figure 1.1)

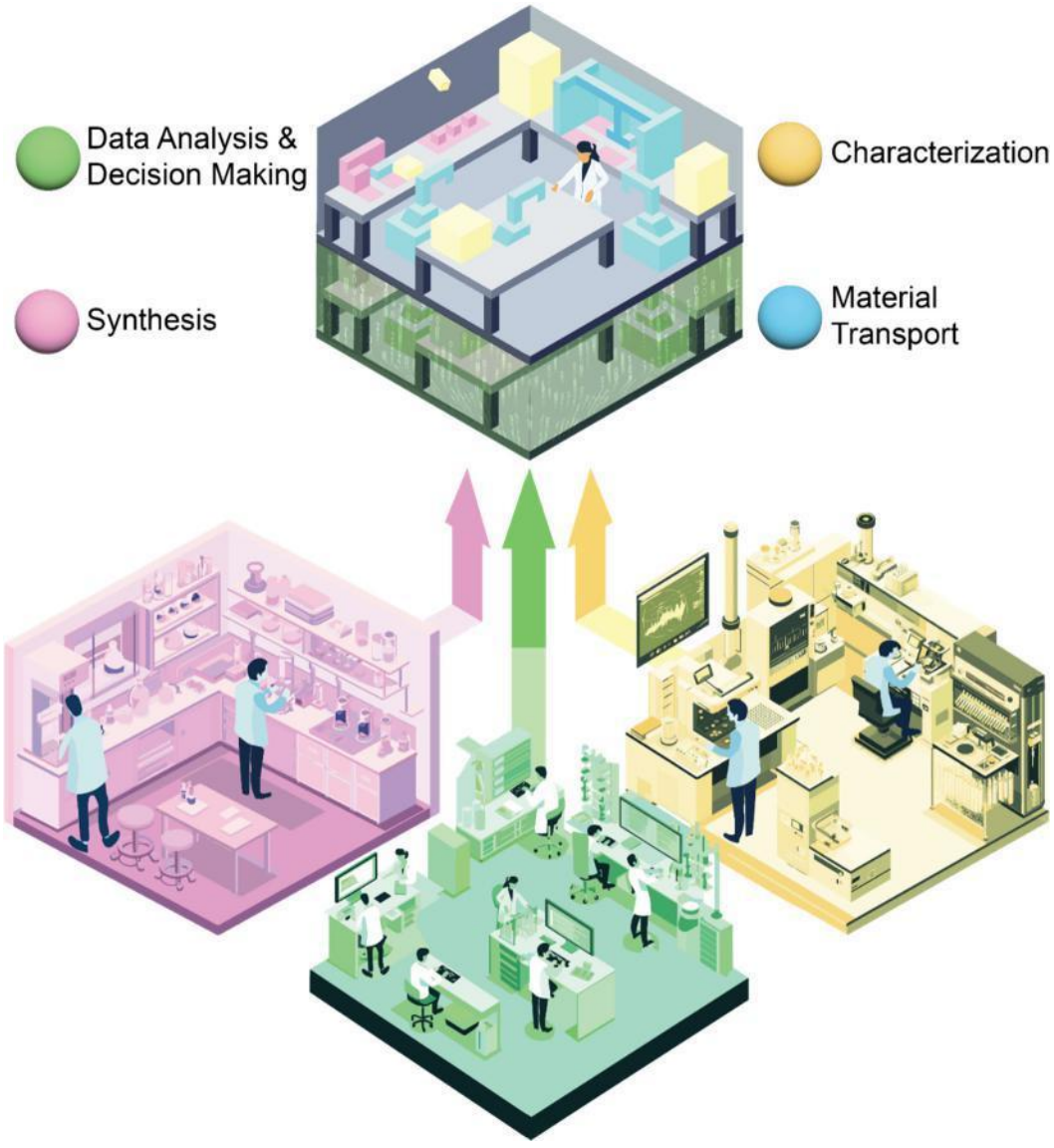

Figure 1.1: Self-Driving Lab Architecture

Combining human expertise with AI agents for decision-making can improve the dimensional chemical spaces that would otherwise be intractable.[2] The AI agent's decision-efficiency of navigating vast chemical landscapes within SDLs. By refining strategies in real time, the AI agent of SDLs identifies the most promising experimental routes in high- making performance depends on robust, unbiased, and reproducible data. Reliable datasets result from systematically designed experiments, and they guide predictive models. In this way, data and AI form a feedback loop that fuels scientific progress. As Thomas Kuhn observed in The Essential Tension,[4] true scientific breakthroughs often arise not from deeper pattern recognition alone, but from the creative disruption of established frameworks—suggesting that future advances may require new forms of AI or computing, capable of transcending existing paradigms

Extending a chemical engineering analogy, each "process unit" within an SDL should be optimized not only to produce valuable materials but also to generate high-quality, information-rich datasets that enhance the AI agent's predictive power.

1.2 Process Intensification and Its Convergence with Self-Driving Labs

The chemical engineering toolbox includes several frameworks that have transformed the way we design, assess, and improve chemical processes in terms of efficiency, safety, and sustainability. Among the chemical engineering toolboxes, Process Intensification (PI) stands out as a systematic framework influencing all scales of chemical engineering innovations. A process can be viewed as any task or series of tasks necessary to accomplish a goal, in the traditional chemical engineering standpoint; such tasks can be categorized by scale or by unit operations or "process units" (e.g., storage, transport, mixing, separation, reaction, characterization, etc.). Intensifying a process translates to achieving intended goals with drastically enhanced performance while minimizing required resources – such as materials, time, and capital – or any

other relevant process metric. Taken holistically, PI has driven the development of novel equipment, methods, and their synergistic integrations across different scales.[5] In this Comment article, we briefly discuss how to harness PI principles for designing resource-efficient SDLs for a given research problem.

The classical vision of PI has been established through four fundamental principles:

1. Maximizing the effectiveness of intra- and intermolecular events,
2. Giving each molecule the same processing experience (uniform reaction conditions),
3. Optimizing driving forces while maximizing specific surface areas,
4. Maximizing synergistic effects from partial processes.

These principles are traditionally achieved through four fundamental approaches in different domains: structure (spatial), energy (thermodynamic), synergy (functional), and time (temporal).[5] The convergence of SDLs and PI gives rise to the concept of data intensification. Through the iterative nature of SDLs' closed-loop decision-making, data intensification strategies lead to substantial improvements in experimental data quality across multiple metrics: amount (volume), rate (cost per data), reliability (precision), and scope (capability space coverage). Data utility and efficiency can be drastically improved from the standard gridded-domain search by employing AI-guided optimization campaigns which leverage prior knowledge that influences a decision-making policy to propose a next experiment (or trajectory of experiments) that increases the likelihood of meeting a task's goal (or objective). Furthermore, data itself could be considered both an approach to and an outcome of PI – better data enables better understanding and control of molecular events, processing conditions, driving forces, and synergistic effects, which in turn generates higher quality data for its decision-making "process unit." (Figure 1.2).

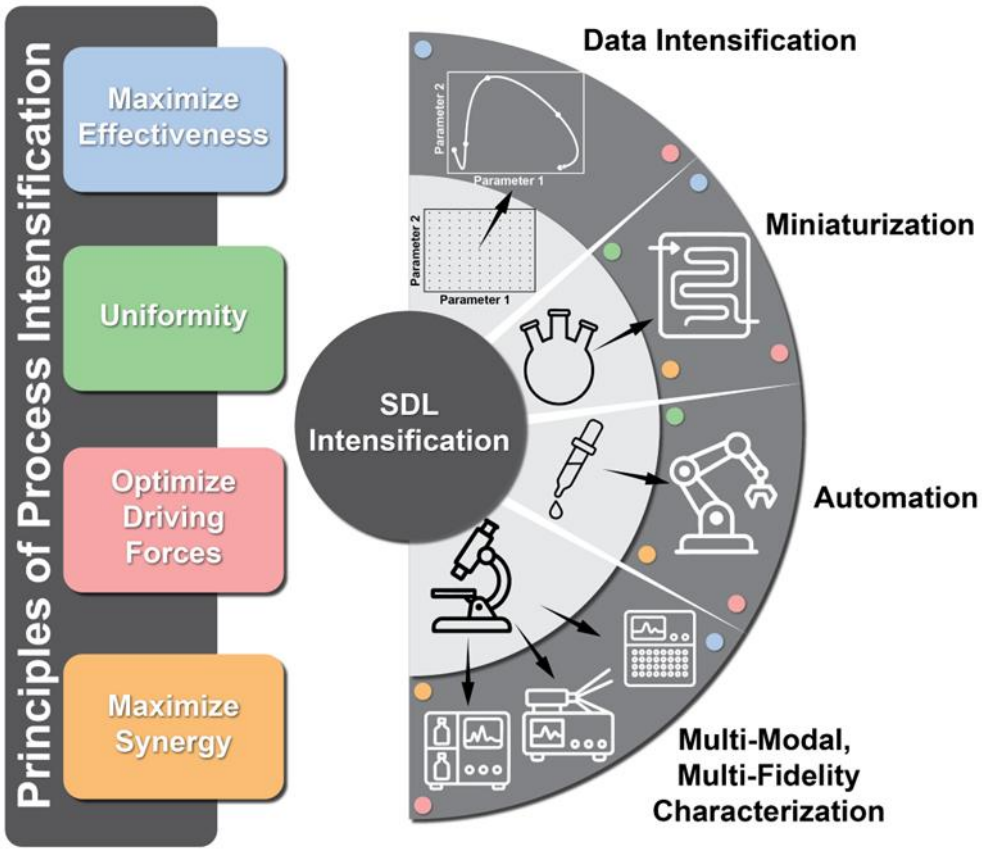

Figure 1.2: Intensification of SDL Process Units

SDLs designed by chemical engineering principles leverage the PI frameworks through integration of the four fundamental approaches – structure, energy, synergy, and time – to optimize experimental workflows and accelerate research. When rate-limiting phenomena are identified in a reaction "process unit" – whether mass transfer, heat transfer, reaction kinetics, or photon flux – these are addressed through the optimization of driving forces and enhancement of specific surface areas.[6] A prime example is the widespread adoption of microreactor technology across SDLs, from materials discovery to pharmaceutical process development. These miniaturized reactors (Figure 1.2) reduce reaction volumes from milliliters to microliters while providing unprecedented control over reaction conditions through enhanced heat and mass transfer rates. The high surface-to-volume ratio of microreactors enables rapid mixing and efficient heat transfer, leading to improved yields and selectivities. Furthermore, parallelization of miniaturized batch reactors

allows for faster chemical domain exploration in micro-well plate reactors, while continuous flow synthesis can exploit transient data to approximate steady-state conditions thanks to instantaneous changes in process parameters.[7] When integrating the intensified reactor unit with the characterization unit, one should choose a characterization timescale that matches the upstream process, to avoid a bottleneck in the SDL workflow. To achieve this, most SDLs choose a multi-modal and multi-fidelity strategy (Figure 1.2), combining rapid in-situ measurements for real-time decision-making with more detailed ex-situ characterization for comprehensive material analysis.[8] This approach allows for rapid screening and process control while still gathering the detailed data needed for fundamental studies and validation. PI-empowered SDLs can reduce materials and molecular discovery and development timelines by orders of magnitude compared to the status quo while minimizing resource consumption and waste generation.[9]

1.3 Modularity, Standardization, and the Future of Sustainable SDLs

When a process requires workup steps such as washing, separation, or other pre/post-treatments, SDLs can benefit from maximizing synergistic effects between partial processes through integration and simplification of process units. For example, AlphaFlow, a self-driven fluidic lab that combines droplet-based microfluidics, in-line phase separation, and real-time analytics for autonomous multi-step synthesis, exemplifies this integration.[10] AlphaFlow was tasked with the discovery and optimization of colloidal atomic layer deposition (cALD) – a precision synthesis technique for growing hetero-nanostructures with monolayer control. AlphaFlow's transport "process unit" was controlled through modular fluidic micro-processors enabling seamless integration of formulation, synthesis, characterization, and phase separation operations within an end-to-end, automated workflow (Figure 1.2). Using reinforcement learning (RL), AlphaFlow autonomously explored and optimized a 40-dimensional parameter space,

consuming less than one five-hundredth of the materials required by conventional methods while generating data at a rate equivalent to over 100 researchers working simultaneously. Without any prior knowledge of conventional cALD sequences, AlphaFlow discovered a novel, more efficient multi-step synthetic route that achieved superior optical properties compared to literature protocols. AlphaFlow exemplifies how the convergence of PI principles with autonomous experimentation can lead to improved material properties and more sustainable, intensified research practices in SDLs.

While the introduction of intensified technologies into SDLs has accelerated scientific research, the design, building, and implementation of SDLs remain slow. This bottleneck stems from the diverse requirements and unique complexities of process units needed for specific research goals. The lack of standardized process units has undermined PI's widespread adoption and consequently hindered SDL development cycles. Modularity, a complementary concept to PI, offers a solution through reconfigurable process units that can be readily integrated and adapted.[11] Such process units, whether off-the-shelf commercial solutions or retrofitted low-cost units, must share common interfaces and protocols to enable rapid assembly of new SDLs and modification of existing ones. Achieving this goal is facilitated by open innovation initiatives (e.g., open-sourcing and expertise sharing) from researchers worldwide to democratize their SDLs hardware and software modules.

Beyond hardware considerations, data handling and processing must follow modular principles. Modular intensified SDL deployment enables successful, distributed, and decentralized SDL networks capable of tackling complex research objectives. Each intensified process (sub-) module must comply with all PI principles. Giving all molecules the same processing experience is particularly crucial, as it ensures reproducibility across SDLs sharing standard (sub-)modules.

This standardization is exemplified in a distributed continuous flow chemistry-based SDLs, where pharmaceutically relevant aldol condensation reaction across different locations with a shared commercial reactor module was explored.[12]

For bespoke SDLs, reproducibility requires comprehensive documentation of the fundamental PI approaches employed in each (sub-)module, including structural (standard molecular descriptors and reactor geometry), thermodynamic (form, amount, moment, and position of applied energy field), functional (data-driven models of the synergistic effects), and temporal (dynamic states, periodicity, or continuous processing characteristics) domains of intensification. Recent work has demonstrated how a standardized chemical language can facilitate the transfer of experimental instructions for batch systems.[13] Such standardized frameworks and abstractions could enable knowledge transfer while maintaining the benefits of PI across diverse SDL implementations.[14]

This Comment explored PI as a foundational framework for designing sustainable SDLs, but broader chemical engineering principles, including circular chemistry, must also be integrated to maximize the SDLs' impact. Moving beyond a linear trajectory, SDLs should embrace a sustainable, closed-loop model that accounts for not only efficiency gains but also auxiliary material consumption, waste reduction, and resource regeneration. Achieving this vision necessitates rethinking both hardware and software paradigms—developing modular, reusable, and reconfigurable process units while establishing standardized experimental workflows and data architectures. A concerted effort within the chemical engineering community is essential to implement common standards that enable seamless knowledge transfer across SDLs, ensuring that intensification strategies remain scalable and adaptable. By treating both physical resources and experimental data as co-products of scientific discovery, SDLs can leverage data intensification to

maximize knowledge extraction—where even transient, previously discarded data can inform decision-making with minimal system reconfiguration. This holistic integration of PI and sustainability principles will accelerate scientific breakthroughs and create a globally connected network of SDLs that democratize access to powerful research capabilities.[15] If successfully implemented, PI-empowered SDLs will serve as a scalable blueprint for sustainable research acceleration across chemical engineering and beyond, demonstrating how foundational principles can drive technological progress while safeguarding planetary integrity

1.4 Study Objectives and Overview of Dynamic Flow Experiment Strategy

To address limitations in data utilization and to fully leverage the dynamic capabilities of flow-based synthesis platforms, this work introduces Dynamic Flow Experiments (DFEs) as a data intensification strategy for accelerated materials discovery. Building upon prior developments in flow chemistry and transient experimentation, this study presents the first systematic application of DFEs for inorganic materials synthesis, using colloidal cadmium selenide (CdSe) quantum dots (QDs) as a model system, which was inspired by dynamic flow experiments for organic synthesis.[16], [17], [18], [19], [20], [21], [22], [23], [24], [25], [26]

The DFE strategy aims to transform underutilized transient states into high-resolution data by continuously varying a key process parameter—residence time—during synthesis. As illustrated in Figure 1.3, DFE enables the collection of a complete system response trajectory during continuous operation, in contrast to steady-state flow experiments (SSFEs), which capture only a single equilibrium point after stabilization.

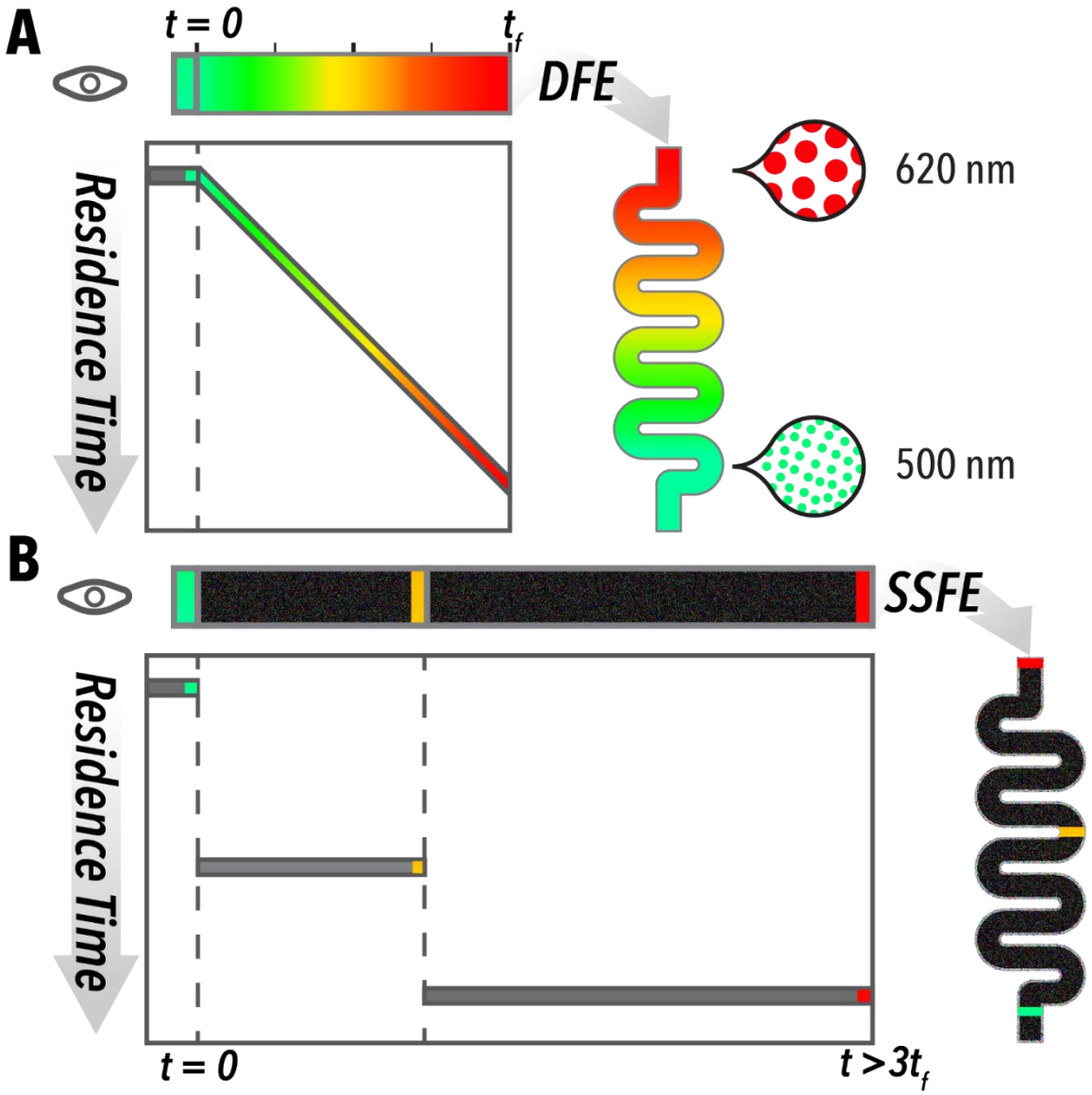

Figure 1.3: (A) Dynamic vs (B) Steady State Flow Experiment

Through real-time integration of in-situ characterization tools (e.g., UV-Vis and PL spectroscopy), the transient data collected in DFEs can be mapped to their steady-state equivalents, enabling enhanced model development and decision-making. This data-rich methodology offers three major benefits:

1. Increased data throughput — each DFE yields significantly more data points than a corresponding SSFE with equivalent material and time constraints.

2. Reduced material consumption — continuous sampling throughout an experiment lowers precursor use by up to threefold.
3. Accelerated exploration of synthesis conditions — DFEs span a wide range of conditions in a single run, drastically reducing total experimentation time.

To demonstrate the utility of this approach in an autonomous setting, this study integrates DFE with a Self-Driving Fluidic Lab (SDFL) equipped for real-time sensing, automated control, and machine learning–guided experiment planning. Specifically, the objectives of this work are to:

- Develop and validate a DFE protocol for high-temperature CdSe QD synthesis.
- Establish a method for mapping transient synthesis trajectories to steady-state material properties.
- Demonstrate the use of DFE as a model initialization tool for Bayesian Optimization (BO) algorithms.
- Execute a full autonomous synthesis and optimization campaign to target desired quantum dot properties using DFEs.

This framework establishes a scalable and sustainable methodology for high-resolution, autonomous exploration of synthesis–property relationships in emerging materials systems.

Chapter 2 : ACCELERATED SYNTHESIS SPACE MAPPING OF INORGANIC NANOMATERIALS WITH DATA-RICH EXPERMIMENTATION

2.1 Chemicals

Perfluorinated oil (PFO, 97%), cadmium oxide (CdO, > 99.9%), selenium powder (Se, >99.99%), oleic acid (OA, 90%), 1-octadecene (ODE, 90%), and trioctylphosphine (TOP, 90%), anhydrous toluene (Tol, 99.8%), acetone (>99.5%), Sudan blue II (98%) were procured from Sigma Aldrich and used as received.

2.2 Cadmium Precursor Preparation

CdO powder (1027 mg), ODE (375 mL), and OA (25 mL) were added into a 500 mL round bottom flask. The solution was vacuumed for 1 h at 150 °C until the solution was transparent. The transparent solution was placed under nitrogen purging for 1 h at 190 °C. The solution was then transferred into the glove box for storage

2.3 Selenium Precursor Preparation

Se Powder (632 mg), TOP (10 mL), and ODE (390 mL) were added to a 500 mL round bottom flask inside a glove box. The solution was stirred overnight to become a colorless solution and left in the glove box until use.

2.4 Data-Rich SDFL Hardware

The developed SDFL is composed of different physical and digital modules: fluid delivery, reaction, characterization, control, and inference. The fluid delivery module consisted of five computer-controlled syringe pumps (Chemyx Fusion 6000) loaded with air-tight stainless-steel syringes of 20 mL and 100 mL (Chemyx) for precursors and ODE, respectively. The reaction module was fabricated using stainless steel (SS) tubing (0.0625″ outer diameter (OD) × 0.03″ inner diameter (ID), IDEX U-190). The module combined a 300 μL helical coil with a curvature

diameter (DC) of 25.4 mm to use as preheater of the Se precursor, and a 1113 μL CFI reactor with DC of 3.175 mm. The preheater (T_{pre}) and reaction (T_{rxn}) temperatures were controlled independently via a PID controller (Omega CN8PT-330), the preheater used a single 100 W cartridge heater (Watlow) while each reactor module used two 100 W cartridge heaters. The Cd and Se precursors were diluted with their respective ODE syringe pumps, ODE_{Cd} and ODE_{Se}, to achieve a specific concentration and molar ratio before in-flow injection and mixing. To ensure uniform mixing before entering the flow reactor module, a custom-built braided micromixer (perfluoroalkoxy [PFA] tubing, 0.0625″ OD × 0.03″ ID, Microsolv Technology) was used.[27]

The in-situ characterization module was placed 50 cm (228 μL) downstream of the flow reactor module to allow the as-synthesized QDs enough time to cool down to room temperature before performing in-situ UV-Vis ABS and PL spectroscopy. The in-situ spectral measurements were carried out using a custom-designed three-port flow cell connected to a fiber-coupled broadband light source (BAL 2000, Ocean Insight), a fiber-coupled LED (365 nm, Thorlabs), and a miniature UV-Vis spectrometer (HDX spectrometer, Ocean Insight). 30 measurements of UV-Vis absorption and PL spectra were captured in sequence at 1.5 s intervals, with 6 ms and 3 ms integration times, respectively.

LabVIEW (National Instruments version 24.0) was used for the control module of the entire hardware of the developed SDFL. The process control module of the SDFL coordinates the operation of the flow reactor and preheater temperatures, T_{rxn} and T_{pre}, respectively; the LED and UV-vis light sources; and the spectrometer and syringe pump flow rates. The inference module consisted of a custom-developed Python script that parses the raw spectral measurements generated by the SDFL hardware to later be used to retrain the surrogate AI model and subsequently suggest new experiments via a single-objective Bayesian optimization (BO)

framework, thus closing the loop of the SDFL. Detailed information on the integration of the control and inference modules can be found in Appendix A.

2.5 QD Purification

For ex-situ characterization of the autonomously synthesized CdSe QDs, the as-synthesized QDs were washed using an antisolvent precipitation method. First, acetone was added as an antisolvent to the as-synthesized CdSe QD dispersion in a 1:1 volume ratio. The mixture was then centrifuged at 10,000 rpm for 10 min to separate the precipitated CdSe QDs. The collected precipitate was re-dispersed in toluene. A second round of washing was performed using acetone as the antisolvent, followed by centrifugation at 10,000 rpm for 10 min. Finally, the precipitate was collected and re-dispersed in 1 mL of toluene for further characterization.

2.6: Ex-situ Characterization

X-ray diffraction (XRD) and grazing incidence X-ray diffraction (GIXRD) were used to characterize the samples. The washed QD dispersion was drop-cast onto glass substrates. GIXRD were performed using a Rigaku SmartLab X-ray Diffractometer (Cu Kα source, 1.54 Å, 44 mA, 40 kV) in Bragg-Brentano and parallel beam configurations, respectively. Transmission electron microscopy (TEM) images were obtained from FEI Talos F200X (200 kV).

2.7 Experimental Platform for Dynamic Synthesis of Quantum Dots

To implement Dynamic Flow Experiments (DFEs) for accelerated materials discovery, we developed a Self-Driving Fluidic Lab (SDFL) designed for the high-temperature, continuous synthesis of colloidal quantum dots (QDs). This automated platform integrates precise fluidic control, real-time data acquisition, and autonomous feedback systems within a closed-loop architecture, enabling high-resolution mapping of synthesis conditions to material properties. [7]

In this study, we targeted the synthesis of cadmium selenide (CdSe) quantum dots using a hot-injection flow chemistry protocol. The experimental workflow begins with the controlled dilution and preheating of precursor solutions, followed by in-flow mixing, reaction, and in-situ optical analysis. The synthesis process is governed by six key parameters, summarized in Table 2.1.

Table 2.1: Controlled Variables in the SDFL Synthesis Platform

Parameter	Definition
X_1	Volumetric flow rate ratio of Cd precursor to ODE_{Cd} (Cd / ODE_{Cd})
X_2	Volumetric flow rate ratio of Se precursor to ODE_{Se} (Se / ODE_{Se})
X_3	Volumetric flow ratio between total Cd stream and total Se stream (Cd:Se)
T_{pre}	Preheater temperature applied to the Se precursor stream before merging
T_{rxn}	Reaction temperature inside the microreactor where QD nucleation and growth occur
τ	Residence time of the fluid inside the microreactor, controlling exposure time and growth rate

The synthetic workflow begins with the preparation of cadmium and selenium precursor streams. The Cd precursor (cadmium oxide in 1-octadecene) is diluted in flow by adjusting the volumetric flow ratio of cadmium to its diluent (X_1). Similarly, the Se precursor (selenium in trioctylphosphine and ODE) is preheated and diluted using ODE_{Se}, defined by the volumetric ratio X_2. These precursor streams are then combined in flow at a defined inter-precursor ratio (X_3), triggering the nucleation of nanocrystals. The combined stream is directed through a Coiled Flow Inverter (CFI) microreactor, where particle growth occurs over a controlled residence time (τ) at the reaction temperature T_{rxn}. Upon exiting the reactor, the mixture is cooled to room temperature and passed through a three-port flow cell for in-situ UV-Vis and PL spectroscopy, with measurements collected every 3 seconds. All spectral data are time-stamped, enabling exact correlation between material properties and the synthesis conditions experienced by each fluid

segment. These data streams are automatically processed by a custom Python script, which extracts relevant optical features (e.g., λ_{em}, FWHM), updates the digital twin of the system, and provides input for closed-loop optimization algorithms. A detailed schematic of the SDFL hardware and the dynamic flow synthesis workflow is presented in Figure 2.1, highlighting the modular integration of fluid handling, reaction, and real-time characterization modules [7].

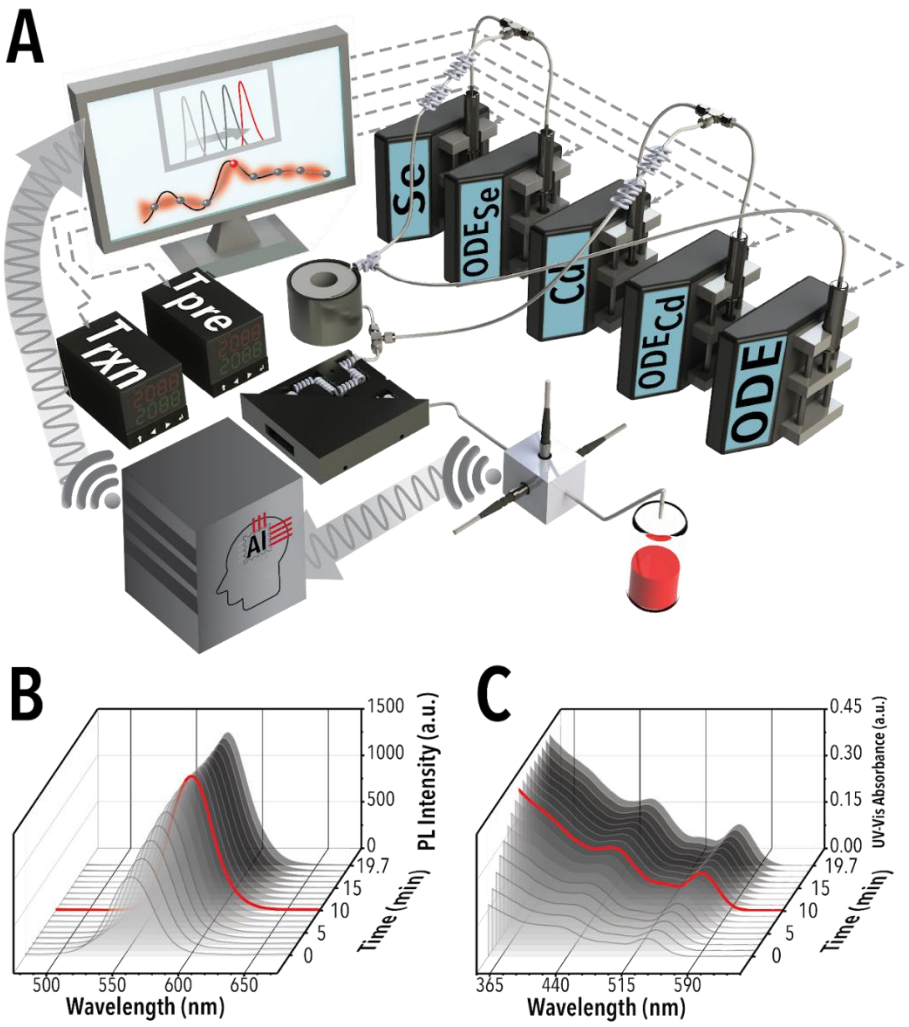

Figure 2.1: Experimental Setup. Overview of the developed SDFL for data-intensified parameter space exploration of CdSe QDs. (A) Schematic illustration of the SDFL hardware for continuous autonomous synthesis of CdSe QDs. An example of the in-situ obtained UV-Vis (B) photoluminescence and (C) absorption spectra of the in-flow synthesized QDs

2.8 Reactor Design and Flow Characterization

The success of DFE relies on low-uncertainty knowledge about the time each fluidic element spends inside the microreactor and its corresponding optical features.[7] To reduce the uncertainty of the DFE to steady-state flow experiment (SSFE) mapping, it is critical to ensure that each fluidic element experiences a uniform chemical environment (e.g., no radial gradients) and that adjacent elements experience distinct process parameters (e.g., minimal axial dispersion)—i.e., a plug-flow reactor. Flow reactor engineering plays an important role in obtaining a narrow residence time distribution (RTD), i.e. near plug flow conditions, ensuring narrow axial dispersion along the flow direction. The plug flow behavior and mixing efficiency in a microreactor are influenced by geometric parameters and volumetric flow rates .[28]

A coiled flow inverter (CFI) geometry was adapted for the SDFL microreactor. The CFI design creates near plug-flow conditions through passive mixing, enabling reliable dynamic sampling and reproducible results during the DFE operation. A set of RTD experiments was conducted to study the plug-flow behavior of the CFI microreactor. The CFI microreactor was designed to promote the development of secondary flow (intensified mixing). CFI curvature ratio ($\lambda = Dc / Di$) plays an important role in controlling the plug-flow behavior of the microreactor. Large λ inhibits the appearance of the secondary flow as it would approach the behavior of a straight tube.[29] The CFI design utilized in this study had a $\lambda < 10$ [30] with 90° bends and three to four coiled turns for each 90° bend [29], [31], [32]. A photograph and schematic of the CFI microreactor are shown in Figure 2.2. Further details on the geometric parameters of the CFI used in this study are summarized in Table 2.2

Table 2.2: CFI Microreactor Geometry and Operating Condition

Parameter	Description	Value
Inner diameter (Di)	Internal diameter of the reactor tubing	0.762 mm
Curvature diameter (Dc)	Diameter of curvature in coiled sections	3.175 mm
Curvature ratio (λ)	Promotes the development of secondary Dean flow	<10
Turns per bend	Promotes intensified mixing	3-4 turns
Reactor volume (V_r)	Defined from reactor geometry	1113 μL

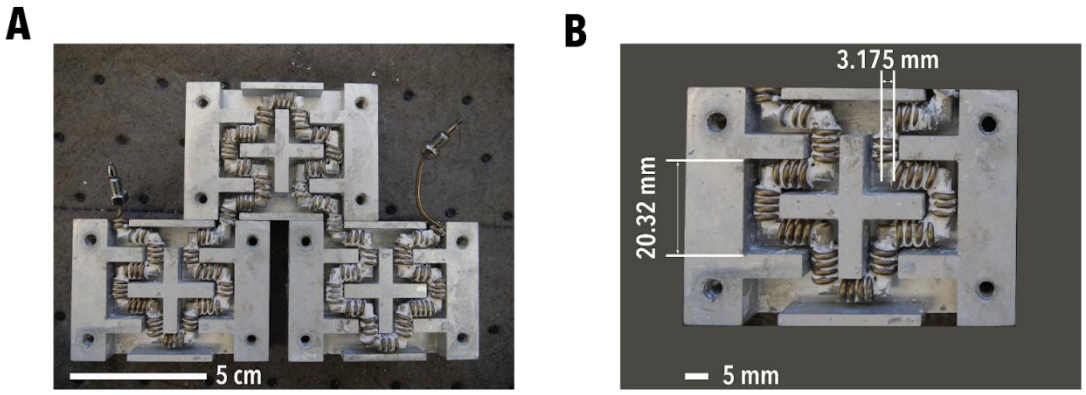

Figure 2.2: Schematic of the CFI Microreactor

The dimensionless Bodenstein number (Bo) was utilized as the primary metric to characterize the plug-flow dispersion [29]. The results of the RTD experiments demonstrated that the designed CFI microreactor achieves plug flow conditions within the DFE operational envelope. Detailed information about the RTD experiment can be found in Appendix B.

Table 2.3: RTD Results and Plug-Flow Assessment

Nominal Residence Time (τ)	Measured Average τ	Bodenstein Number (Bo)	Flow Regime
0.5 min	0.5 min	301.8	Near plug flow
9 min	8.7 min	216.5	Near plug flow

The experimentally determined Bo numbers were 301.8 and 216.5 for residence times of 1 min and 9 min, respectively (Table 2.3). These Bo values significantly exceed the threshold for plug

flow behavior, confirming that the flow reactor operates in a near-ideal plug flow regime under the experimental conditions investigated

2.9 DFE Protocol and Residence Time Mapping

Once the plug-flow behavior of the SDFL microreactor was established, the fundamentals of the DFE process for inorganic material synthesis were investigated. The developed DFE process involves three steps:

1. The fluidic platform runs for three microreactor volumes (V_r) until steady state has been reached at a short initial residence time (τ_o), typically set to 1 min.
2. A linear ramp of residence time begins with a specific slope (α).
3. The DFE continues until the instantaneous residence time (τ_{ins}) reaches a predetermined final residence time (τ_f).

The evolution of residence time during the dynamic ramp is expressed as:

$$\tau_{ins} = \tau_0 + \alpha \cdot t \quad \text{(Equation 1)}$$

The mapping between measurement time (t_m) and the expected steady-state equivalent residence time (τ) follows a derivation adapted from Moore and Jensen[25]:

$$\tau = (1 - e^{-\alpha}) e^{-\frac{V_d}{V_r}\alpha} \left(t_m + \frac{\tau_0}{\alpha} \right) \quad \text{(Equation 2)}$$

Equation 2 accounts for the dead volume (V_d) and the residence time profile the reactive system experiences inside the microreactor during the start of a new DFE. The slope α was informed by the prior work of Florit and Jensen and maintained constant at $\alpha = 0.6$ [33].

This protocol allows the DFE process to continuously traverse the parameter space while recording data at every intermediate condition, which is later mapped to its equivalent steady-state condition using the above transformation. The process enables data intensification, where high-resolution synthesis–property relationships can be established with minimal experimental time and

material consumption. Detailed information about the DFE vs SSFE mapping can be found in Appendix C

2.10 Reproducibility and Comparison with SSFEs

To assess the reproducibility of the SDFL hardware during the DFE process, four identical DFEs were performed under a constant QD synthesis condition (X_1 = 0.30, X_2 = 0.27, X_3 = 0.73, T_{pre} = 227°C, T_{rxn} = 284°C). The mean values and standard deviations from the DFE runs were compared with results from seven steady-state flow experiments (SSFEs) conducted under matching synthesis conditions at discrete residence times of 1–7 minutes. Figure 2.3A and Figure 2.3B demonstrate that DFE accurately captures quantum dot (QD) properties — including emission wavelength (λ_{em}) and full width at half maximum (FWHM) with an error of less than 1%. Furthermore, all SSFE results fall within two standard deviations of the DFE ramp experiments. The standard deviation in Figure 2.3A–B is attributed to day-to-day variation in the precursors (e.g., precursor aging and batch-to-batch variation)

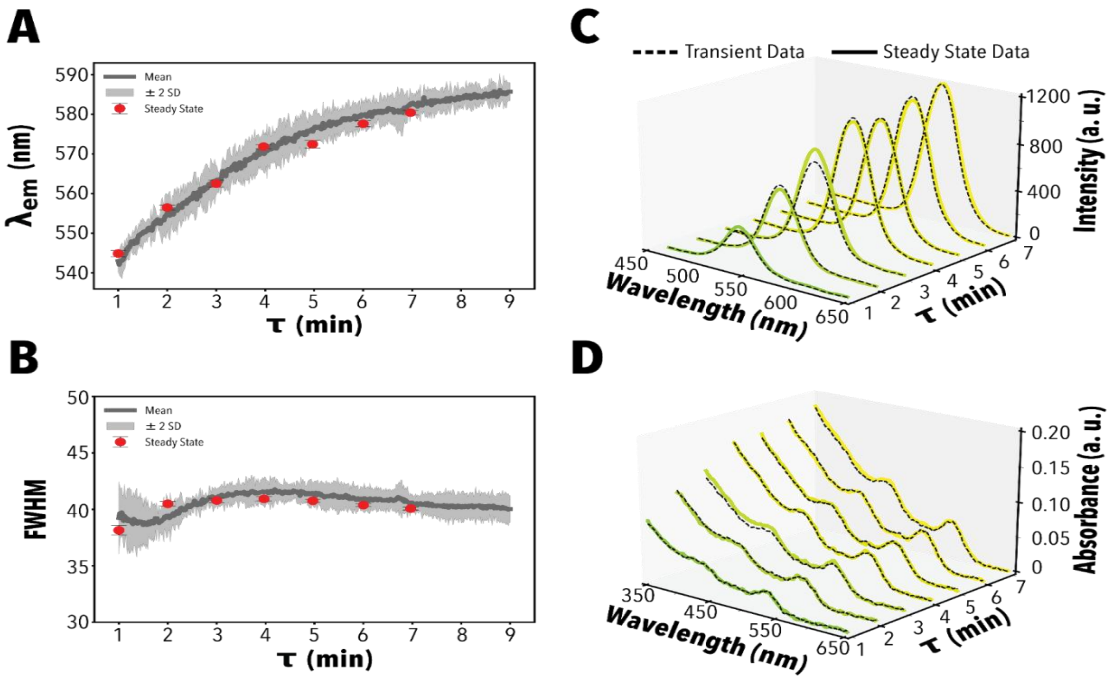

Figure 2.3: DFE vs SSFE

Figure 2.3C and Figure 2.3D benchmark the complete UV-Vis ABS and PL spectra of in-flow synthesized CdSe QDs obtained from DFE against their expected SSFE equivalents. The comparison confirms the validity of the mapping between dynamic and steady-state residence times and supports the near plug-flow behavior in the microreactor.

The validated DFE-to-SSFE mapping enables accurate extraction of QD properties such as:

- λem,
- FWHM,
- First excitonic peak wavelength,
- PL area,
- Absorbance at excitation.

These results demonstrate that DFE can serve as a material- and time-efficient alternative to SSFE without compromising on accuracy or reproducibility.

2.11 Autonomous Workflow and DFE-LHS Sampling

The development of a data-rich experimentation methodology to capture any SSFE reaction condition within the residence time range of an arbitrary DFE becomes highly beneficial in active learning strategies, where machine learning (ML) model initialization data can be expensive to collect. The lack of prior knowledge, or training data is a well-known challenge in materials acceleration platforms [34].

Common sampling strategies for unknown material synthesis parameter spaces include grid[35], Sobol[36], or Latin hypercube sampling (LHS)[37], [38] . When combined with DFE, these techniques yield a significantly richer initial dataset. For example, an initialization budget of

15 experiments in SSFE provides 15 distinct data points, while DFE can provide at least 720 unique experimental data points in the same duration (assuming 10 s time intervals).

The integration of DFE with LHS introduces a data intensification strategy into a sampling technique constructed to maximize sparsity and representation of each component in a high-dimensional design space [39]. This strategy accelerates the exploration of complex synthesis spaces, as demonstrated in autonomous CdSe QD synthesis campaigns.

Figure 2.4 illustrates the SDFL operation workflow for autonomously mapping the formulation–synthesis–properties relationship of CdSe QDs:

- A human user defines the target λ_{em} and loads initial QD precursors into the SDFL.
- The SDFL automatically performs DFE-LHS experiments, generating a high quantity of high-quality experimental data.
- This data serves to initialize a surrogate model, which is used in subsequent closed-loop optimization via Bayesian Optimization (BO).

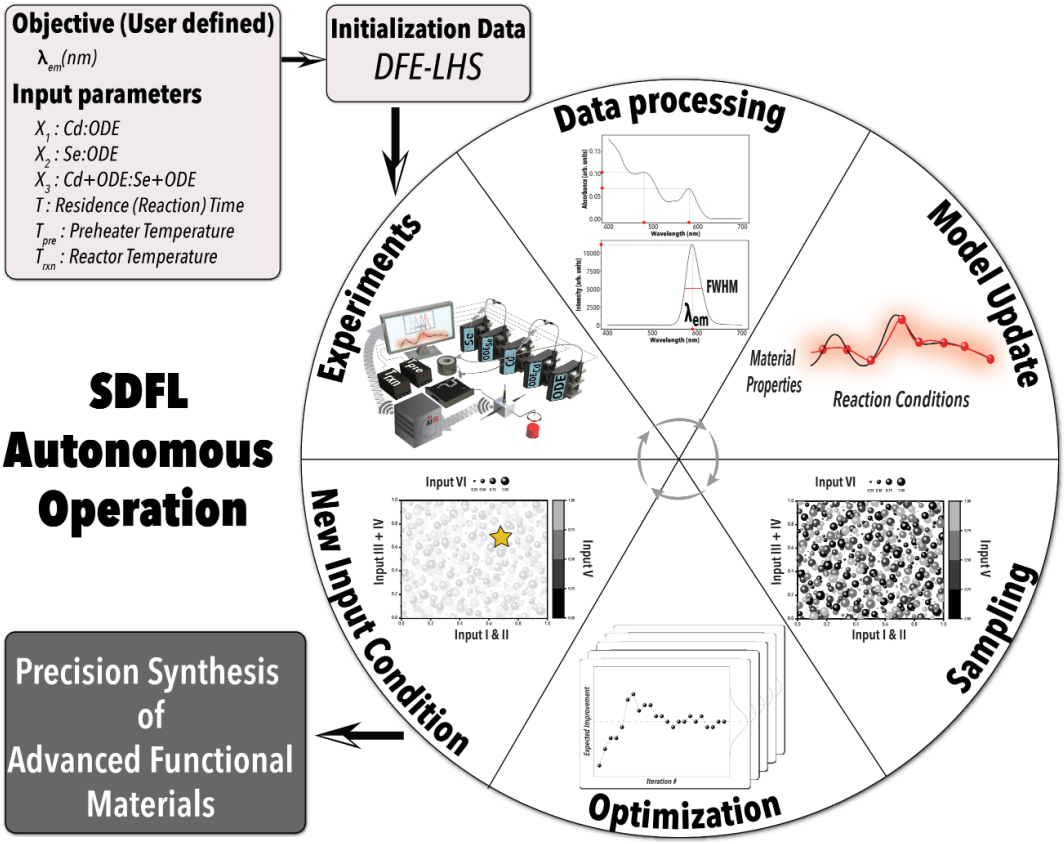

Figure 2.4: SDFL Operation Workflow

The initialization data included 15 LHS experiments from a 5D input parameter space (excluding residence time τ, which was automatically explored via DFE). The advantage of DFE-LHS over SSFE under the same experimental budget is detailed in Appendix D.

A scalarization approach was used to balance target λ_{em} and QD quality (FWHM). Weights of 87.5% (λ_{em}) and 12.5% (FWHM) were assigned to reflect that 1 nm improvement in λ_{em} is seven times more important than 1 nm improvement in FWHM. This scalarized objective function was used throughout the BO optimization process.

2.12 Digital Twin Model and SHAP Analysis

The Gaussian Process Regression (GPR) model was trained using the automatically generated DFE-LHS experimental data. This ML model served two purposes:

1. A surrogate model for subsequent autonomous Bayesian Optimization (BO) synthesis campaigns of CdSe QDs.
2. A digital twin of the SDFL, which accurately predicts QD properties — emission wavelength (λ_{em}) and FWHM — with $R^2 > 0.95$.

A digital twin is a virtual representation of a physical system that mirrors its behavior and performance based on real-time data and machine learning models. In this context, the SDFL digital twin enables accurate predictions of CdSe QD properties under varying synthesis conditions, providing a powerful tool for simulating and optimizing experimental outcomes without additional physical experimentation.

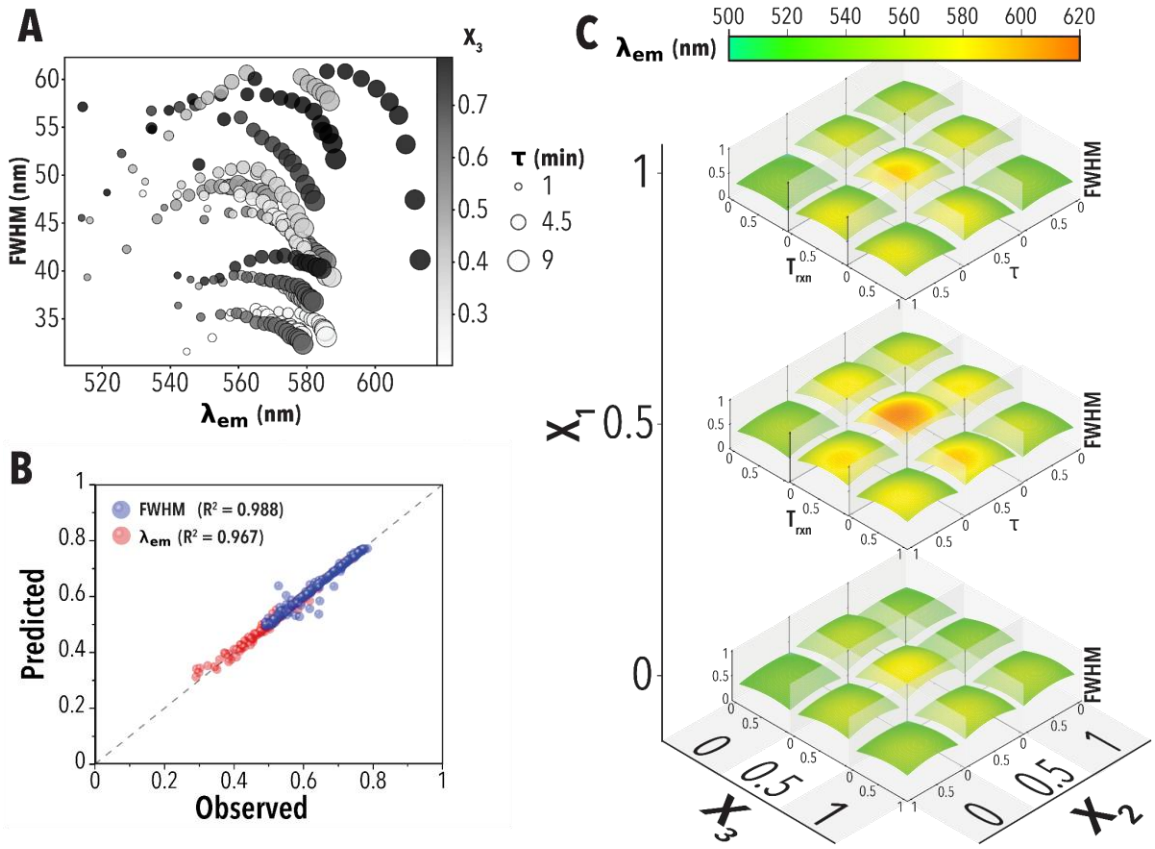

Figure 2.5: DFE Sampling Results

Figure 2.5A presents the results of the DFE-LHS of high-temperature colloidal CdSe QD synthesis using the developed SDFL. The output parameter space is visualized by plotting λ_{em}

versus FWHM, and each point is colored by the cadmium-to-selenium dilution flow ratio (X_3), using a grayscale gradient. This shows the broad distribution of synthesized quantum dot properties resulting from different LHS-selected input combinations, all evaluated under dynamic flow conditions.

Figure 2.5B shows the parity plot from a 5-fold cross-validation of the GPR model used as the digital twin. The strong correlation between predicted and experimental values for both λ_{em} and FWHM confirms the predictive accuracy of the model, further validating its use in autonomous optimization campaigns. The digital twin can reliably forecast material properties in untested regions of the synthesis parameter space, enabling simulation-driven decision making in the closed-loop workflow.

To visualize the power of the digital twin trained on high-quality experimental data, surface plots were generated across the design space, shown in Figure 2.5C. λ_{em} and FWHM are plotted as a function of reactor temperature (T_{rxn}) and residence time (τ) across different values of X_1, X_2, and X_3 at a fixed preheater temperature (T_{pre}). These plots reveal a consistent trend:

Short residence times and low reaction temperatures result in smaller nanocrystals, while longer residence times and higher reaction temperatures promote larger particle growth. This behavior aligns with classical nucleation and growth theory, where both temperature and reaction time significantly impact nanocrystal size and optical properties.[40], [41], [42]

The high prediction accuracy of the SDFL digital twin enabled the precise identification of key synthesis parameters through Shapley Additive Explanations (SHAP) analysis [43]. SHAP analysis is a game-theoretic approach that attributes change in the predicted outcome to individual input features. By quantifying the contribution of each synthesis parameter to the model's

predictions, SHAP analysis enhances model interpretability and reveals how different variables influence QD properties.

Refer to Appendix E, SHAP analysis identified:

- For λ_{em}: residence time (τ), cadmium dilution (X_1), and reactor temperature (T_{rxn}) were the most influential parameters.
- For FWHM: T_{rxn}, selenium dilution (X_2), and X_1 were the dominant features.

2.13 Optimization Campaigns and On-Demand Synthesis

To demonstrate the practical advantages of the DFE technique as a data-rich machine learning model initialization strategy, four autonomous CdSe QD synthesis campaigns were conducted using the developed SDFL. Each campaign employed a single-objective Bayesian Optimization (BO) algorithm to target specific emission wavelengths of 540 nm, 560 nm, 580 nm, and 600 nm, with an experimental budget of 10 steady-state experiments.

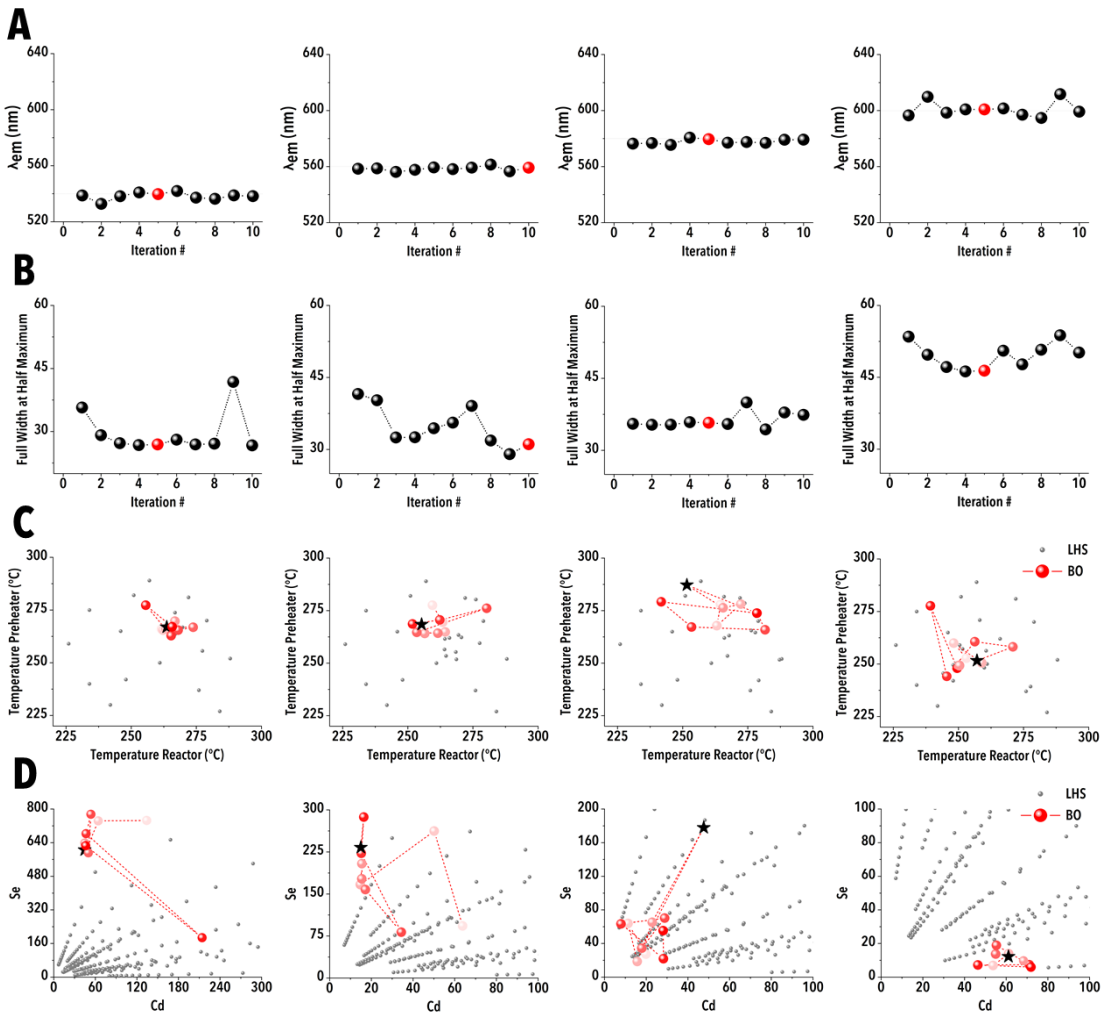

Figure 2.6: BO Campaigns Targeting different Peak Emission Wavelength of CdSe QDs

Figure 2.6A and Figure 2.6B illustrate the progression of λ_{em} and FWHM across the 10 BO iterations for each target emission wavelength. The BO algorithm alternated between exploration (using the Expected Improvement acquisition policy) and pure exploitation (using Upper Confidence Bound with $\beta = 0$) at iterations 5 and 10, balancing the trade-off between learning new regions of the parameter space and refining high-performing conditions.

- In all four campaigns, the BO algorithm identified the target λ_{em} in the first iteration, demonstrating the effectiveness of the DFE-LHS-initialized surrogate model.

- In three out of four cases (540 nm, 580 nm, and 600 nm), the narrowest FWHM at the target λ_{em} was achieved by the fifth iteration.
- The 560 nm campaign required all 10 iterations, illustrating the BO agent's ability to navigate more complex regions of the parameter space.

These results confirm that a DFE-initialized surrogate model can efficiently guide autonomous experimentation toward both accurate emission targets and high material quality (low FWHM).

Figure 2.6C shows the reactor and preheater temperatures explored by the BO algorithm throughout each campaign. The algorithm dynamically adjusted T_{rxn} and T_{pre} to identify the optimal synthesis pathways for each λ_{em} target.

Figure 2.6D presents the evolution of the cadmium-to-selenium volumetric flow ratio (Cd/Se) sampled across the BO iterations. The BO agent explored a range of Cd/Se ratios within predefined limits, progressively refining the precursor mixing conditions to improve QD quality and match target optical properties.

Together, Figure 2.6C and Figure 2.6D demonstrate the efficient exploration of the multi-dimensional synthesis space by the SDFL BO framework, powered by the data-intensified initialization provided by DFE-LHS.

These optimization campaigns highlight several important outcomes. First, all four autonomous experiments demonstrated early convergence to the target emission wavelengths, with the desired λ_{em} reached as early as the first iteration in each case. Second, the workflow was cost- and time-efficient, leveraging the accuracy of the DFE-LHS-initialized surrogate model to significantly reduce the number of required physical trials. Finally, the results validate the scalability and robustness of the DFE-LHS approach when applied to high-dimensional parameter spaces, confirming its ability to autonomously synthesize high-quality colloidal quantum dots with

precise optical characteristics. These campaigns validate the DFE-integrated SDFL as a powerful platform for closed-loop autonomous optimization, with broad applicability across emerging materials systems.

2.14 Continuous Manufacturing and Structural Characterization

The structure and morphology of the autonomously manufactured CdSe QDs by the SDFL were characterized by using transmission electron microscopy (TEM) and X-ray diffraction (XRD) (Figure 2.7A and Appendix F).

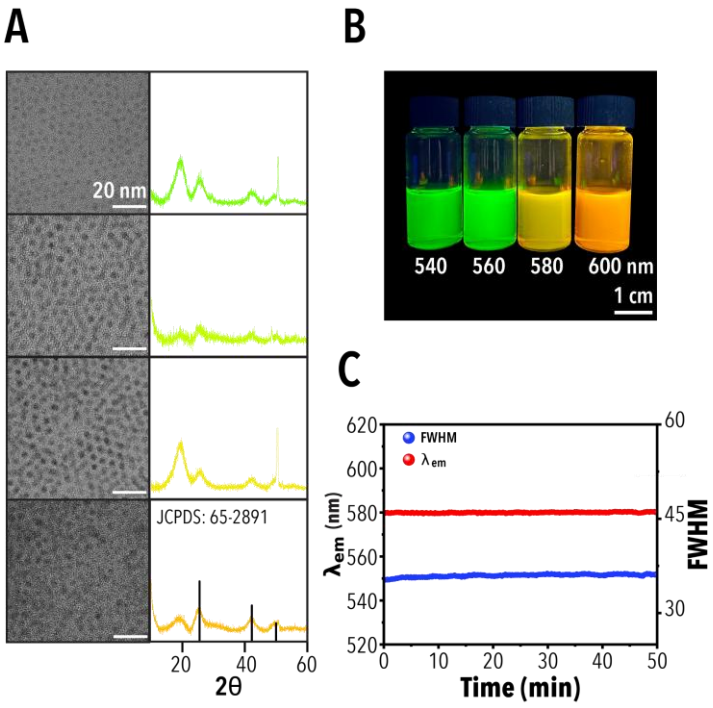

Figure 2.7: Continuous Manufacturing of CdSe QDs

Figure 2.7A shows XRD and TEM characterization of the as-synthesized CdSe QDs with the SDFL. From top to bottom, λ_{em} = 540 nm, 560 nm, 580 nm, and 600 nm, respectively.

Figure 2.7B shows images of 20 mL CdSe QD samples under UV illumination at different target λ_{em} values. The as-synthesized QDs' λ_{em} was within 0.35% of the target value over the course of a 50-minute continuous flow manufacturing run (Figure 2.7C and Appendix F).

As illustrated in Figure 2.7C, the autonomously optimized QDs can be continuously manufactured with a narrow λ_{em} and FWHM variance (coefficient of variance <0.2% for λ_{em} and <3% for FWHM, respectively). Figure 2.7C presents the temporal variation of λ_{em} and FWHM over 50 min of the continuous manufacturing run at λ_{em} = 580 nm using the synthetic route autonomously discovered by the SDFL (Refer to Appendix F for the other target λ_{em}).

Chapter 3 : CONCLUSIONS AND FUTURE WORK

3.1 Summary of Findings

This work directly addresses the core challenges of high-dimensional parameter space exploration and optimization in materials research, where efficiently generating, analyzing, and integrating large datasets is essential for rapid innovation. By producing a robust and representative mapping of the synthesis landscape early on, DFEs enable more confident decision-making of ML agents and significantly reduce the risk of overlooking critical synthesis pathways. This is especially crucial for emerging materials systems, where intricate interdependencies among process variables, precursor chemistries, and property outcomes often necessitate iterative, data-driven optimization strategies.

Using CdSe QDs as a testbed, we comprehensively validated the precision and reliability of the DFE approach, demonstrating a strong correlation between transient and steady-state synthesis conditions. The resulting high-fidelity dataset underscores the potential of DFEs to substantially advance the discovery, optimization, and production of functional materials while upholding sustainability principles. Moreover, we demonstrated the potential of integrating DFEs with BO workflows to further enhance the research acceleration capabilities of SDFLs, paving the way for a transformative evolution in data-driven materials innovation and manufacturing. By incorporating a DFE-driven BO initialization strategy for an SDFL, our approach achieves a significantly accelerated and more sustainable route for exploring advanced functional materials in previously unexplored parameter spaces. Remarkably, the entire cycle—from initial sampling to continuous manufacturing of the target inorganic materials—can be completed within a single day, leveraging the data-rich prior knowledge provided to the SDFL's ML agent. This synergy of

DFEs and SDFLs sets a new benchmark for scalable, sustainable, and intelligent materials discovery, development, and manufacturing processes.

3.2 Future Work

While this study focused on ramping residence time as a primary strategy for data intensification, future work could explore the use of dynamic trajectories through other synthesis parameters, such as precursor concentration and temperature. Varying precursor concentrations in a controlled dynamic fashion could provide additional insight into reactivity regimes and precursor ratio optimization for different quantum dot systems.

Dynamic ramping of temperature, although more complex, presents an intriguing opportunity for further exploration. However, temperature ramps introduce unique challenges due to the thermal gradient effects along the reactor, which can influence nucleation and growth rates non-linearly. These gradients may lead to non-uniform growth environments across fluidic elements, complicating the mapping between transient and steady-state conditions. Careful engineering of reactor heating profiles and real-time thermal feedback may be required to address such non-idealities.

Another avenue for future development involves replacing the traditional steady-state experimentation used in Bayesian Optimization (BO) campaigns with fully dynamic experimental trajectories. Instead of conducting discrete BO iterations at constant synthesis conditions, dynamically varying input parameters—guided by the surrogate model—could allow for more data-dense exploration and faster convergence. This approach would further maximize the efficiency of SDFLs by continuously feeding high-resolution, structured data into the optimization pipeline without requiring steady-state holds.

Such extensions would deepen the capabilities of DFEs in materials research and bring the field closer to real-time, autonomous control over synthesis pathways for increasingly complex material systems.

REFERENCES

[1] L. Persson *et al.*, "Outside the Safe Operating Space of the Planetary Boundary for Novel Entities," *Environ. Sci. Technol.*, vol. 56, no. 3, pp. 1510–1521, Feb. 2022, doi: 10.1021/acs.est.1c04158.

[2] M. Abolhasani and E. Kumacheva, "The rise of self-driving labs in chemical and materials sciences," *Nat. Synth.*, vol. 2, no. 6, Art. no. 6, Jun. 2023, doi: 10.1038/s44160-022-00231-0.

[3] F. Strieth-Kalthoff *et al.*, "Delocalized, asynchronous, closed-loop discovery of organic laser emitters," *Science*, vol. 384, no. 6697, p. eadk9227, May 2024, doi: 10.1126/science.adk9227.

[4] T. S. Kuhn, *The Essential Tension: Selected Studies in Scientific Tradition and Change*. Chicago, IL: University of Chicago Press, 1979. Accessed: Apr. 15, 2025. [Online]. Available: https://press.uchicago.edu/ucp/books/book/chicago/E/bo5970650.html

[5] T. Van Gerven and A. Stankiewicz, "Structure, Energy, Synergy, Time—The Fundamentals of Process Intensification," *Ind. Eng. Chem. Res.*, vol. 48, no. 5, pp. 2465–2474, Mar. 2009, doi: 10.1021/ie801501y.

[6] T. Savage, N. Basha, J. McDonough, J. Krassowski, O. Matar, and E. A. del Rio Chanona, "Machine learning-assisted discovery of flow reactor designs," *Nat. Chem. Eng.*, vol. 1, no. 8, pp. 522–531, Aug. 2024, doi: 10.1038/s44286-024-00099-1.

[7] J. D. Williams, P. Sagmeister, and C. O. Kappe, "Dynamic flow experiments for data-rich optimization," *Curr. Opin. Green Sustain. Chem.*, vol. 47, p. 100921, Jun. 2024, doi: 10.1016/j.cogsc.2024.100921.

[8] A. E. Siemenn *et al.*, "Using scalable computer vision to automate high-throughput semiconductor characterization," *Nat. Commun.*, vol. 15, no. 1, p. 4654, Jun. 2024, doi: 10.1038/s41467-024-48768-2.

[9] M. A. McDonald, B. A. Koscher, R. B. Canty, J. Zhang, A. Ning, and K. F. Jensen, "Bayesian Optimization over Multiple Experimental Fidelities Accelerates Automated Discovery of Drug Molecules," *ACS Cent. Sci.*, vol. 11, no. 2, pp. 346–356, Feb. 2025, doi: 10.1021/acscentsci.4c01991.

[10] A. A. Volk *et al.*, "AlphaFlow: autonomous discovery and optimization of multi-step chemistry using a self-driven fluidic lab guided by reinforcement learning," *Nat. Commun.*, vol. 14, no. 1, p. 1403, Mar. 2023, doi: 10.1038/s41467-023-37139-y.

[11] B. P. MacLeod, F. G. L. Parlane, A. K. Brown, J. E. Hein, and C. P. Berlinguette, "Flexible automation accelerates materials discovery," *Nat. Mater.*, vol. 21, no. 7, pp. 722–726, Jul. 2022, doi: 10.1038/s41563-021-01156-3.

[12] J. Bai *et al.*, "A dynamic knowledge graph approach to distributed self-driving laboratories," *Nat. Commun.*, vol. 15, no. 1, p. 462, Jan. 2024, doi: 10.1038/s41467-023-44599-9.

[13] S. H. M. Mehr, M. Craven, A. I. Leonov, G. Keenan, and L. Cronin, "A universal system for digitization and automatic execution of the chemical synthesis literature," *Science*, vol. 370, no. 6512, pp. 101–108, Oct. 2020, doi: 10.1126/science.abc2986.

[14] R. B. Canty and M. Abolhasani, "Reproducibility in automated chemistry laboratories using computer science abstractions," *Nat. Synth.*, vol. 3, no. 11, pp. 1327–1339, Nov. 2024, doi: 10.1038/s44160-024-00649-8.

[15] D. A. Boiko, R. MacKnight, B. Kline, and G. Gomes, “Autonomous chemical research with large language models,” *Nature*, vol. 624, no. 7992, pp. 570–578, Dec. 2023, doi: 10.1038/s41586-023-06792-0.
[16] J. P. McMullen and B. M. Wyvratt, “Automated optimization under dynamic flow conditions,” *React. Chem. Eng.*, vol. 8, no. 1, pp. 137–151, Dec. 2022, doi: 10.1039/D2RE00256F.
[17] C. A. Hone, N. Holmes, G. R. Akien, R. A. Bourne, and F. L. Muller, “Rapid multistep kinetic model generation from transient flow data,” *React. Chem. Eng.*, vol. 2, no. 2, pp. 103–108, Apr. 2017, doi: 10.1039/C6RE00109B.
[18] S. Mozharov *et al.*, “Improved Method for Kinetic Studies in Microreactors Using Flow Manipulation and Noninvasive Raman Spectrometry,” *J. Am. Chem. Soc.*, vol. 133, no. 10, pp. 3601–3608, Mar. 2011, doi: 10.1021/ja1102234.
[19] C. P. Haas, S. Biesenroth, S. Buckenmaier, T. van de Goor, and U. Tallarek, “Automated generation of photochemical reaction data by transient flow experiments coupled with online HPLC analysis,” *React. Chem. Eng.*, vol. 5, no. 5, pp. 912–920, May 2020, doi: 10.1039/D0RE00066C.
[20] L. Schrecker *et al.*, “Discovery of unexpectedly complex reaction pathways for the Knorr pyrazole synthesis via transient flow,” *React. Chem. Eng.*, vol. 8, no. 1, pp. 41–46, Dec. 2022, doi: 10.1039/D2RE00271J.
[21] K. C. Aroh and K. F. Jensen, “Efficient kinetic experiments in continuous flow microreactors,” *React. Chem. Eng.*, vol. 3, no. 1, pp. 94–101, Feb. 2018, doi: 10.1039/C7RE00163K.
[22] C. Waldron, A. Pankajakshan, M. Quaglio, E. Cao, F. Galvanin, and A. Gavriilidis, “Model-based design of transient flow experiments for the identification of kinetic parameters,” *React. Chem. Eng.*, vol. 5, no. 1, pp. 112–123, Dec. 2019, doi: 10.1039/C9RE00342H.
[23] J. V. Herck *et al.*, “Operator-independent high-throughput polymerization screening based on automated inline NMR and online SEC,” *Digit. Discov.*, vol. 1, no. 4, pp. 519–526, Aug. 2022, doi: 10.1039/D2DD00035K.
[24] J. Van Herck and T. Junkers, “Rapid Kinetic Screening via Transient Timesweep Experiments in Continuous Flow Reactors,” *Chemistry–Methods*, vol. 2, no. 1, p. e202100090, 2022, doi: 10.1002/cmtd.202100090.
[25] J. S. Moore and K. F. Jensen, “‘Batch’ Kinetics in Flow: Online IR Analysis and Continuous Control,” *Angew. Chem. Int. Ed.*, vol. 53, no. 2, pp. 470–473, Jan. 2014, doi: 10.1002/anie.201306468.
[26] F. Florit *et al.*, “Dynamic flow experiments for Bayesian optimization of a single process objective,” *React. Chem. Eng.*, vol. 10, no. 3, pp. 656–666, Feb. 2025, doi: 10.1039/D4RE00543K.
[27] R. W. Epps, A. A. Volk, K. Abdel-Latif, and M. Abolhasani, “An automated flow chemistry platform to decouple mixing and reaction times,” *React. Chem. Eng.*, vol. 5, no. 7, pp. 1212–1217, Jun. 2020, doi: 10.1039/D0RE00129E.
[28] A. G. Kanaris and A. A. Mouza, “Numerical investigation of the effect of geometrical parameters on the performance of a micro-reactor,” *Chem. Eng. Sci.*, vol. 66, no. 21, pp. 5366–5373, Nov. 2011, doi: 10.1016/j.ces.2011.07.044.

[29] S. Klutz, S. K. Kurt, M. Lobedann, and N. Kockmann, “Narrow residence time distribution in tubular reactor concept for Reynolds number range of 10–100,” *Chem. Eng. Res. Des.*, vol. 95, pp. 22–33, Mar. 2015, doi: 10.1016/j.cherd.2015.01.003.
[30] E. López-Guajardo, E. Ortiz-Nadal, A. Montesinos-Castellanos, and K. D. P. Nigam, “Coiled flow inverter as a novel alternative for the intensification of a liquid-liquid reaction,” *Chem. Eng. Sci.*, vol. 169, pp. 179–185, Sep. 2017, doi: 10.1016/j.ces.2017.01.016.
[31] M. Mridha and K. D. P. Nigam, “Coiled flow inverter as an inline mixer,” *Chem. Eng. Sci.*, vol. 63, no. 6, pp. 1724–1732, Mar. 2008, doi: 10.1016/j.ces.2007.10.028.
[32] A. K. Saxena and K. D. P. Nigam, “Coiled configuration for flow inversion and its effect on residence time distribution,” *AIChE J.*, vol. 30, no. 3, pp. 363–368, 1984, doi: 10.1002/aic.690300303.
[33] F. Florit, A. M. K. Nambiar, C. P. Breen, T. F. Jamison, and K. F. Jensen, “Design of dynamic trajectories for efficient and data-rich exploration of flow reaction design spaces,” *React. Chem. Eng.*, vol. 6, no. 12, pp. 2306–2314, Nov. 2021, doi: 10.1039/D1RE00350J.
[34] R. W. Epps *et al.*, “Artificial Chemist: An Autonomous Quantum Dot Synthesis Bot,” *Adv. Mater.*, vol. 32, no. 30, p. 2001626, 2020, doi: 10.1002/adma.202001626.
[35] F. Bateni *et al.*, “Smart Dope: A Self-Driving Fluidic Lab for Accelerated Development of Doped Perovskite Quantum Dots,” *Adv. Energy Mater.*, vol. 14, no. 1, p. 2302303, 2024, doi: 10.1002/aenm.202302303.
[36] B. P. MacLeod *et al.*, “A self-driving laboratory advances the Pareto front for material properties,” *Nat. Commun.*, vol. 13, no. 1, p. 995, Feb. 2022, doi: 10.1038/s41467-022-28580-6.
[37] T. Osterrieder *et al.*, “Autonomous optimization of an organic solar cell in a 4-dimensional parameter space,” *Energy Environ. Sci.*, vol. 16, no. 9, pp. 3984–3993, Sep. 2023, doi: 10.1039/D3EE02027D.
[38] J. Startt, M. J. McCarthy, M. A. Wood, S. Donegan, and R. Dingreville, “Bayesian blacksmithing: discovering thermomechanical properties and deformation mechanisms in high-entropy refractory alloys,” *Npj Comput. Mater.*, vol. 10, no. 1, pp. 1–13, Jul. 2024, doi: 10.1038/s41524-024-01353-z.
[39] M. D. McKay, R. J. Beckman, and W. J. Conover, “A Comparison of Three Methods for Selecting Values of Input Variables in the Analysis of Output from a Computer Code,” *Technometrics*, vol. 21, no. 2, pp. 239–245, 1979, doi: 10.2307/1268522.
[40] C. B. Murray, D. J. Norris, and M. G. Bawendi, “Synthesis and characterization of nearly monodisperse CdE (E = sulfur, selenium, tellurium) semiconductor nanocrystallites,” *J. Am. Chem. Soc.*, vol. 115, no. 19, pp. 8706–8715, Sep. 1993, doi: 10.1021/ja00072a025.
[41] H. Yang, W. Luan, Z. Wan, S. Tu, W.-K. Yuan, and Z. M. Wang, “Continuous Synthesis of Full-Color Emitting Core/Shell Quantum Dots via Microreaction,” *Cryst. Growth Des.*, vol. 9, no. 11, pp. 4807–4813, Nov. 2009, doi: 10.1021/cg900652y.
[42] X. Xue, Y. Huang, Z. Zhuang, F. Huang, and Z. Lin, “Temperature-sensitive growth kinetics and photoluminescence properties of CdS quantum dots,” *CrystEngComm*, vol. 15, no. 24, pp. 4963–4969, May 2013, doi: 10.1039/C3CE40478A.
[43] S. Lundberg and S.-I. Lee, “A Unified Approach to Interpreting Model Predictions,” Nov. 25, 2017, *arXiv*: arXiv:1705.07874. doi: 10.48550/arXiv.1705.07874.

APPENDICES

Appendix A: Automated and Autonomous Workflows

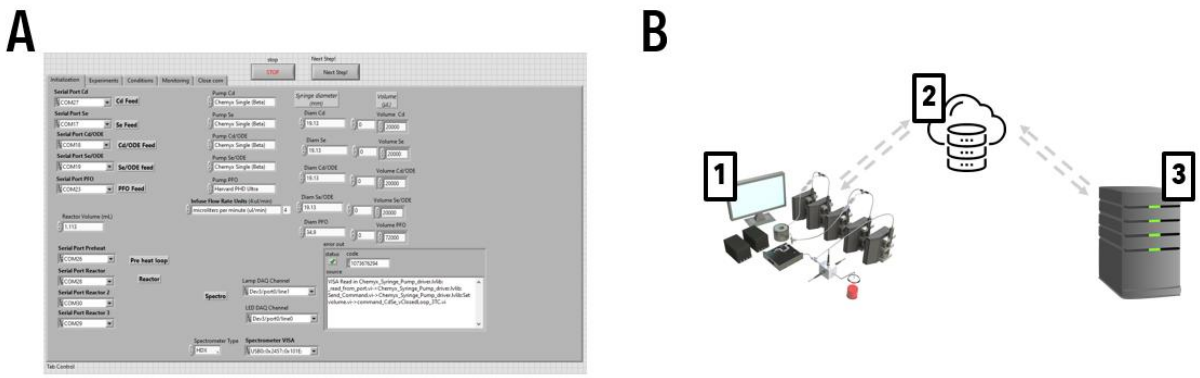

Figure A 1: Developed Workflow for Automated/Autonomous In-Flow QD Synthesis

LabVIEW (National Instruments version 24.0) served as the primary interface for both automated dynamic experimentation and steady-state autonomous optimization process control module. A snapshot of the custom-developed LabVIEW interface is shown in Figure A 1A. Two distinct experimental protocols were implemented. For DFEs, the system accepts a CSV file containing key DFE process parameters: initial and final residence times, ramp duration, corresponding Cd and Se concentrations, and the preheater and microreactor temperatures. For steady-state closed-loop optimization experiments, a separate CSV file specifies individual volumetric flow rates for each precursor syringe (Cd, Se, ODE_{Cd}, and ODE_{Se}) along with the preheater and microreactor temperatures. Both protocols incorporate two configurable waiting periods: a "Residence Time Wait" (specified as a multiple of the nominal residence time) and a "Generic Wait" (specified in minutes). In a typical experimental run, the system undergoes a "Residence Time Wait" factor of 3.5 to ensure steady-state conditions (e.g., a 3.5 min wait for a 1 min residence time condition), followed by a 5-min "Generic Wait" period for sample

collection. Upon completion of these waiting periods (which can be manually overridden), the system flags the next 10 in-situ measurements as steady-state data before proceeding with the experiment (i.e., either volumetric flow rate linear ramp or standby for the next suggested experiment). Between each experimental condition, both protocols execute a temperature stabilization period (ensuring ±1°C from setpoint) during which pure ODE flows through both the preheater and microreactor at 500 µL/min to wash the entire fluidic path, ensuring experiment-to-experiment independence. Data collection begins immediately after the temperature stabilization period is complete. A custom-built Python script processes the acquired raw spectra in real-time (through parallelization), extracting key optical features and uploading them to a MongoDB database (version 8.0.3) where it can be accessed and visualized by authorized users.

The steady-state autonomous optimization workflow integrates both the control module described above and the inference module that is located at an external server, as seen in Figure A 1. At the beginning of each experiment, the control module (Figure A 1B), creates a document specifying the datetime stamp of the start of the run, the experiment number, and the datetime stamp of the start of the given experiment. These documents reside in the cloud in a collection called ‘start_times’. Data that is processed in real-time resides in two distinct collections called ‘spectra_processed’ and ‘parameters’ where key optical features (i.e., λ_{em}, FWHM, absorbance at excitation) and process parameters (i.e., volumetric flow rates and preheater and reactor temperatures) were captured, respectively. Each document in these collections contains information about their ‘experiment’, ‘start_run’, and ‘stability’ flag, which is later used by the inference module to keep track of the current experiment and suggest new experimental conditions based on previously suggested experiments and initialization data.

The BO workflow in the inference module utilizes a Single Task Gaussian Process (radial basis function kernel) for each output parameter (i.e., λ**em** and FWHM). Process inputs and outputs were normalized according to Equations A1–A7. The volumetric flow rate inputs are constructed in such a way that a volumetric flow ratio of 1:5 cannot be exceeded. This threshold was chosen to preserve flow stability. The objective function is constructed as a weighted distance between a target emission wavelength and FWHM, shown in Equation A8. For all experimental campaigns, the objective function weights were constant (15.4 and 1 for the λ_{em} and FWHM, respectively). The target for FWHM was maintained constant at 10 nm, while the λ_{em} was varied as desired.

$$X_1 = \frac{\frac{Cd}{Cd + Cd_{ODE}} - \frac{1}{6}}{\frac{5}{6} - \frac{1}{6}} \quad \text{(Equation A1)}$$

$$X_2 = \frac{\frac{Se}{Se + Se_{ODE}} - \frac{1}{6}}{\frac{5}{6} - \frac{1}{6}} \quad \text{(Equation A2)}$$

$$X_3 = \frac{\frac{Cd + Cd_{ODE}}{Cd + Cd_{ODE} + Se + Se_{ODE}} - \frac{1}{6}}{\frac{5}{6} - \frac{1}{6}} \quad \text{(Equation A3)}$$

$$Tau = \frac{\frac{V_{Reactor}}{Cd + Cd_{ODE} + Se + Se_{ODE}} - 0.5}{10 - 0.5}, \; V_{Reactor} = 1113\ \mu L \qquad \text{(Equation A4)}$$

$$T_{pre} = \frac{T_{preheater} - 220}{290 - 220} \qquad \text{(Equation A5)}$$

$$T_{rxn} = \frac{T_{reactor} - 220}{290 - 220} \qquad \text{(Equation A6)}$$

$$Emmission_{Wavelength} = \frac{Peak\ Emmission_{wavelength} - 450}{670 - 450} \qquad \text{(Equation A7)}$$

$$FWHM = \frac{FWHM - 110}{10 - 110} \qquad \text{(Equation A8)}$$

$$\min_{i \in \{Emission\ Wavelength,\ FWHM\}} - \left|\left| w_i \cdot \left(\overline{Y}_{sample_i} - Y_{target_i} \right) \right|\right|_2^2 \qquad \text{(Equation A9)}$$

Each BO campaign conducted with the SDFL had an experimental budget of 10 steady-state experiments. Expected improvement (EI) was used as the decision-making policy during the BO campaign; however, for experiments 5 and 10 (i.e., halfway through the BO campaign and the last experiment) the decision-making policy was changed to pure exploitation (i.e., upper confidence bound with $\beta = 0$). The new BO-predicted experimental condition is sent by the

inference module to a collection called ‘new_conditions’ at the database, that the control module monitors during standby, and then writes to the CSV file, thus closing the loop.

Appendix B: Residence Time Distribution Experiments

The residence time distribution (RTD) of the designed microreactor was experimentally investigated to characterize the system's flow behavior and evaluate the extent of axial dispersion. RTD experiments were conducted using a step-input methodology where a solution of Sudan Blue II in 1-octadecene (ODE) and pure ODE were separately pumped into a T-mixer (IDEX, U-428) positioned at the inlet of the flow reactor module. The RTD experiments were performed at nominal residence times of 0.5 min and 9 min, covering the boundaries of the volumetric flow rate parameter space studied in this work. Additional verification experiments were conducted at intermediate residence times (1 min, 2 min, and 8 min) to ensure consistent behavior. For each RTD experiment, the system was first allowed to reach a steady state at an initial ratio of pure ODE to Sudan Blue II solution of 3:1, followed by a step change to a new ratio of 1:3 while maintaining a constant total volumetric flow rate. The downstream dispersion of the step change was monitored using in-situ UV-Vis absorption spectroscopy at 647 nm with the same setup described in the main text. All RTD experiments were conducted with the flow reactor maintained at 250 °C, matching typical reaction conditions studied in this work.

The experimental data was transformed into an F-curve by normalizing the detector response from 0 to 1 as a function of time. Subsequently, the F-curve was regressed against the dispersion model (Equation A10) described by Levenspiel using Levenberg-Marquardt Algorithm (curve_fit from Sci-Py package) to determine the Bodenstein number (Bo) and the average residence time (Tavg). The Bodenstein number serves as a metric for deviation of the

flow behavior inside the flow reactor from ideal plug-flow behavior, where values above 100 indicate small deviations from plug flow.

$$F(t^*) = \frac{1}{2}\left[\operatorname{erf}\left(\sqrt{\frac{Bo}{4}}\left(\frac{t}{t_{avg}} - 1\right)\right) + \operatorname{erf}\left(\sqrt{\frac{Bo}{4}}\right)\right]$$

(Equation A10)

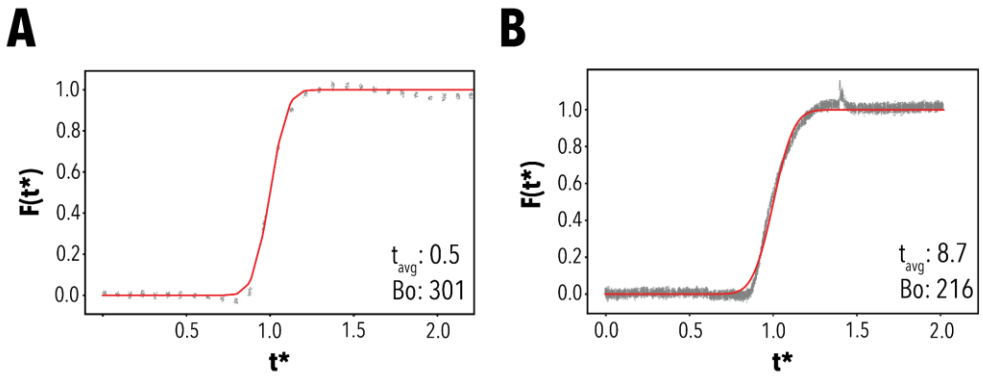

Figure A 2:Residence Time Distribution Experiments

The experimentally determined Bo numbers were 301.8 and 216.5 for residence times of 1 min and 9 min, respectively (Figure A 2). These Bo values exceed the threshold for plug-flow behavior, confirming that the flow reactor operates in a near-ideal plug-flow regime under the investigated experimental conditions. The regressed mean residence times (0.5 min and 8.7 min) showed excellent agreement with the expected nominal residence times (0.5 min and 9 min) calculated from the flow reactor volume and the set volumetric flow rates.

The narrow RTD and high Bo numbers obtained from the RTD experiments can be attributed to the geometry of the flow reactor, which promotes enhanced mixing conditions. The coil flow inverter (CFI) reactor design, used in this work, contains helical coil sections that induce secondary flows, known as Dean flow, arising from the centrifugal forces experienced by the fluid as it traverses the curved path. These secondary flows manifest as counter-rotating vortices perpendicular to the primary flow direction, significantly improving radial mixing.

Additionally, the incorporation of 90-degree bends between coil sections introduces chaotic advection, further enhancing the mixing efficiency. Reactor design parameters such as turns per coiled section (3–4 turns), as well as pitch distance (<4 mm) and curvature ratio (Cr = DC/Di ~ 4) between the diameter of the curvature (DC ~ 3.175 mm) and the diameter of the tube (Di = 0.762 mm), were chosen based on previous literature shown to improve RTD [29], [30], [31], [32]. The CFI microreactor used in this study is shown in Figure 2.2.

Appendix C: DFE vs. SSFE Mapping

The mapping of tm and τ was inspired by the prior work of Moore and Jensen [25]. For completeness, in this section, we provide the correction for small measurement times accounting for dead volume. The measurement time t_m happens once the fluid exits the microreactor and flows through the microreactor dead volume V_d at the outlet. The current flow rate (V_r/Equation 1) and the dead volume give the total time spent in this section. In other words, between the reaction completion time (t_f), or the end residence time ($\tau = t_i - t_f$), and the measurement time, a total volume of V_d must be traversed completely:

$$V_d = \int_{t_f}^{t_m} \frac{V_r}{\tau_0 + \alpha t} dt \qquad \text{(Equation A11)}$$

Solving the integral and dividing by V_r:

$$\frac{V_d}{V_r}\alpha = \ln\left(\frac{\tau_0 + \alpha t_m}{\tau_0 + \alpha t_f}\right) \qquad \text{(Equation A12)}$$

After some manipulation:

$$t_f = e^{-\frac{V_d}{V_r}\alpha} t_m - \left(1 - e^{-\frac{V_d}{V_r}\alpha}\right)\frac{\tau_0}{\alpha} \qquad \text{(Equation A13)}$$

At the start of an DFE, the microreactor undergoes a residence time profile that depends on both the dynamic flow ramp and the previous steady state flow rate. This is because, within the reactor, some fluidic elements would retain the 'memory' of the steady state flow rate at the start of a dynamic volumetric flowrate ramp (t=0)

$$V_r = \int_{t_i}^{0} \frac{V_r}{\tau_0} dt + \int_{0}^{t_f} \frac{V_r}{\tau_0 + \alpha t} dt \qquad \text{(Equation A14)}$$

The first integral corresponds to fluidic elements that have their initial time (t_i) started before the start of the dynamic flow experiment (DFE), hence, their volumetric flow rate is given by the initial residence time (τ_0), and the second integral corresponds to the time they spent under the dynamic experiment ramp, after t = 0, until the end of the reaction time t_f.

Solving the integrals and dividing by V_r:

$$1 = -\frac{t_i}{\tau_0} + \frac{1}{\alpha} \ln\left(\frac{\tau_0 + \alpha t_f}{\tau_0}\right) \qquad \text{(Equation A15)}$$

Solving for t_i:

$$t_i = \tau_0 \left(\frac{1}{\alpha} \ln\left(\frac{\tau_0 + \alpha t_f}{\tau_0}\right) - 1\right) \qquad \text{(Equation A16)}$$

Given the definition of $\tau = t_f - t_i$ and the previous derivation of t_f accounting for dead volume, the mapping for small-times is given by:

$$\tau = e^{-\frac{V_d}{V_r}\alpha} t_m - \left(1 - e^{-\frac{V_d}{V_r}\alpha}\right)\frac{\tau_0}{\alpha} - \tau_0 \left(\frac{1}{\alpha} \ln\left(\frac{\tau_0 + \alpha\left(e^{-\frac{V_d}{V_r}\alpha} t_m - \left(1 - e^{-\frac{V_d}{V_r}\alpha}\right)\frac{\tau_0}{\alpha}\right)}{\tau_0} \right) - 1 \right)$$

(Equation A17)

This correction is applied until the time that the last fluidic element that experiences part of the steady-state (before the dynamic ramp) exits the microreactor (t*). This value has been calculated by Florit et al.,[26]and is given by:

$$t^* = \frac{e^{\alpha\tau_0} - 1}{\alpha} \qquad \text{(Equation A18)}$$

Our implementation considered the small-time regime of τ until it intercepted Equation 2 (main text).

The DFE results were conducted over a duration of approximately 20 min. Applying Equation 2 (main text) with t_m = 20 min results in $\tau_{max} \approx 8.5$ min, enabling continuous sampling across reaction (residence) times ranging from 1 min to 8.5 min. For comparative analysis, a measurement at t_m = 10 min would correspond to a hypothetical steady-state flow experiment (SSFE) with a $\tau \approx 4.65$ min. Allowing for system equilibration (4τ), the complete SSFE parameter-synthesis property mapping requires approximately 18.6 min.

The total material consumption is quantified by integrating the volumetric flow rate over the experimental duration. For SSFE, integration from t = 0 to t = 18.6 min yields 4.5 mL. Similarly, for DFE, integration of the flow rate (calculated as V_r/Equation 1 from the main text) from t = 0 to t_m = 20 min results in 4.758 mL.

The difference in material consumption and processing time between methodologies is ≤ 7%. Notably, the DFE methodology enables continuous synthesis-property mapping across the entire residence time domain (1 min-8.5 min) with temporal resolution of 1 s, offering significantly enhanced sampling density compared to discrete SSFE measurements.

Figure A 3 presents additional results of DFE vs. SSFE benchmarking experiments using the developed SDFL.

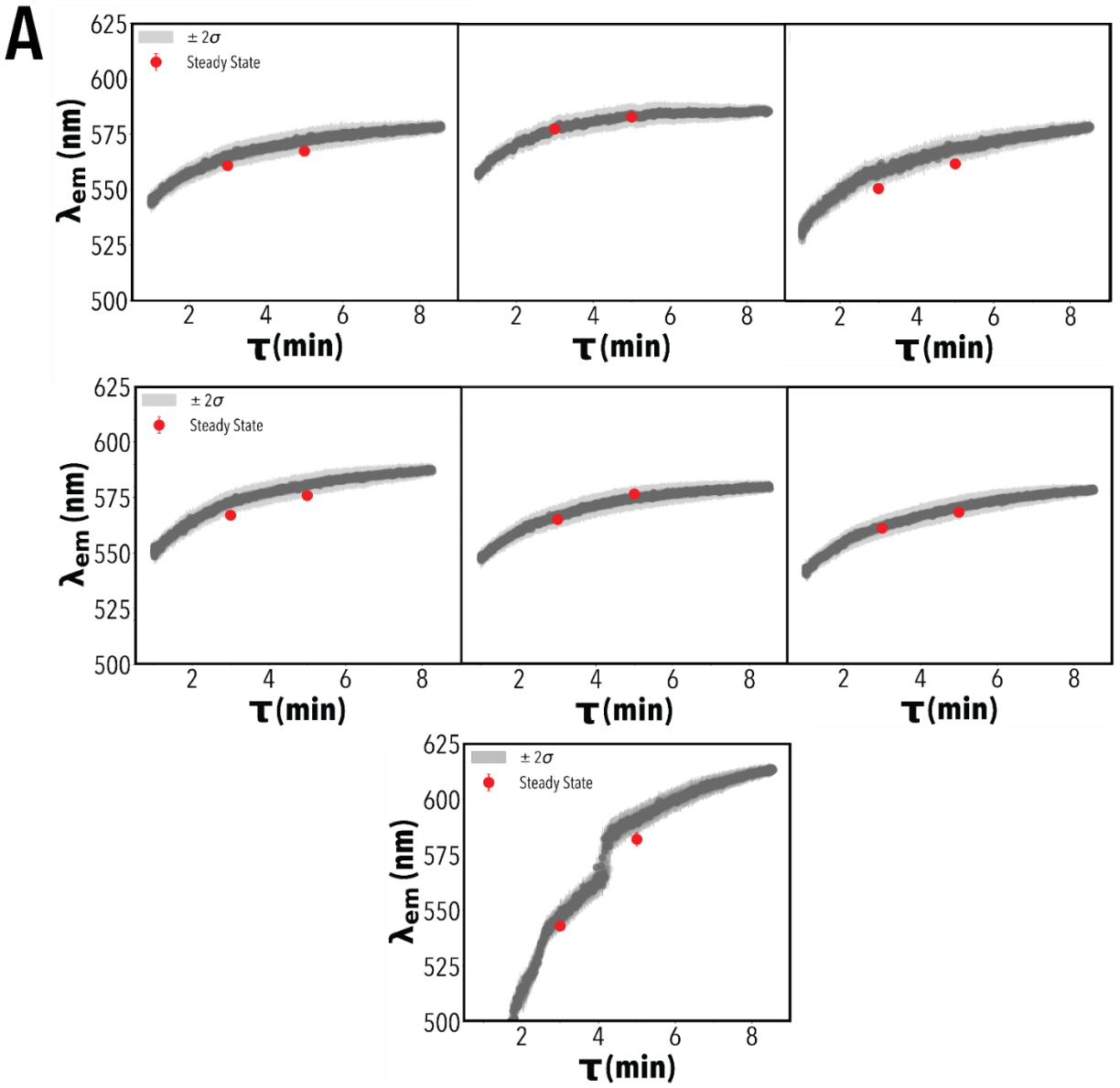

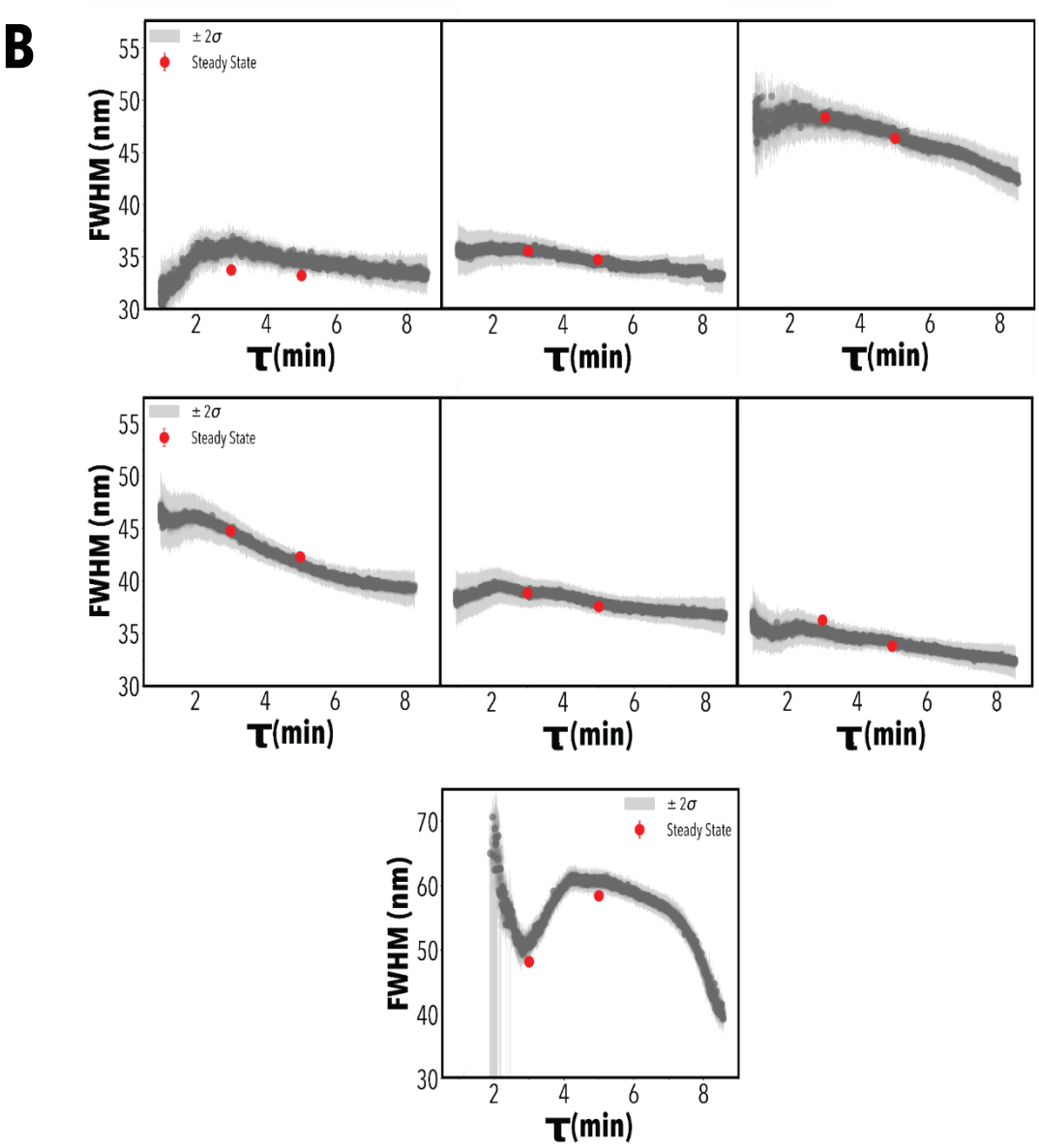

Figure A 3: Transient to Steady State Mapping Validation

Appendix D: Initial Parameter Space Sampling

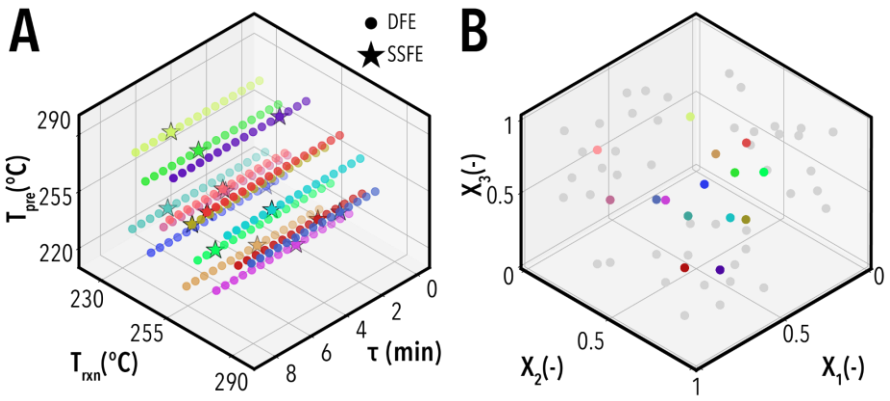

Figure A 4: Latin Hypercube Sampling (LHS) Parameter Space Sampling

Figure A 4 shows the initial sampling of the synthesis parameter space using Latin Hypercube Sampling (LHS). In Figure A 4A, both Dynamic Flow Experiments (DFE, shown as circles) and Steady-State Flow Experiments (SSFE, shown as stars) were performed using 15 initialization experiments. Each point is color-coded based on the values of X_1, X_2 , and X_3, which represent cadmium dilution, selenium dilution, and the Cd/Se flow ratio. Figure A 4B shows the distribution of the LHS samples across the X_1, X_2 , and X_3 space. The light gray dots are projections that help show how well the samples cover the space. This approach gives a good spread of experiments for building machine learning models.

Appendix E: Shapley Additive Explanation Analysis

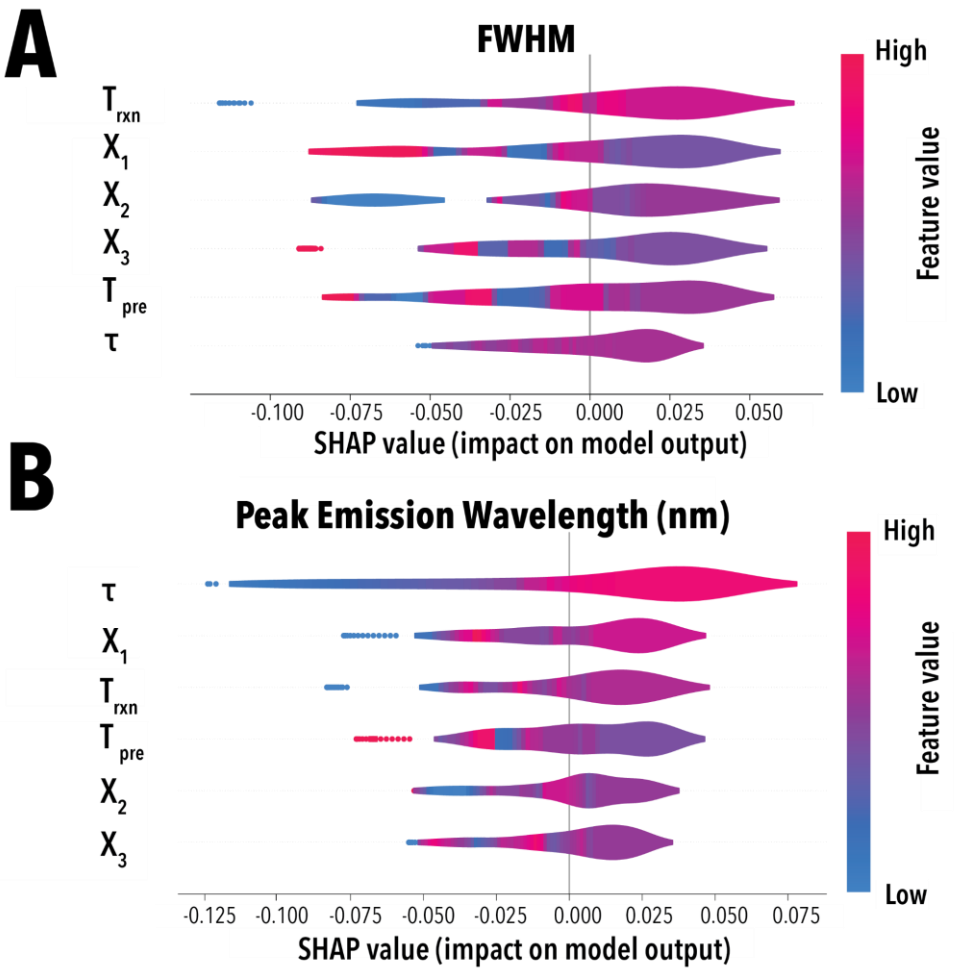

Figure A 5: Shapley Additive Explanation (SHAP) Analysis of the In-Flow CdSe QD Synthesis

Appendix F: Particle Size Distribution from TEM Images and Continuous Nanomanufacturing of the Targeted Wavelength

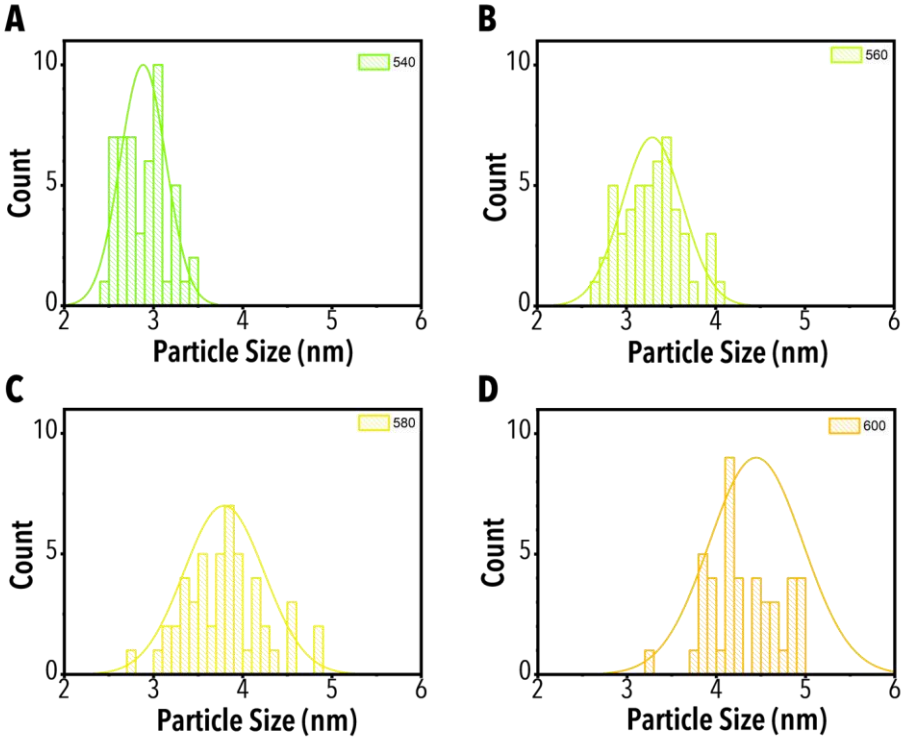

Figure A 6: CdSe QD Size Distribution

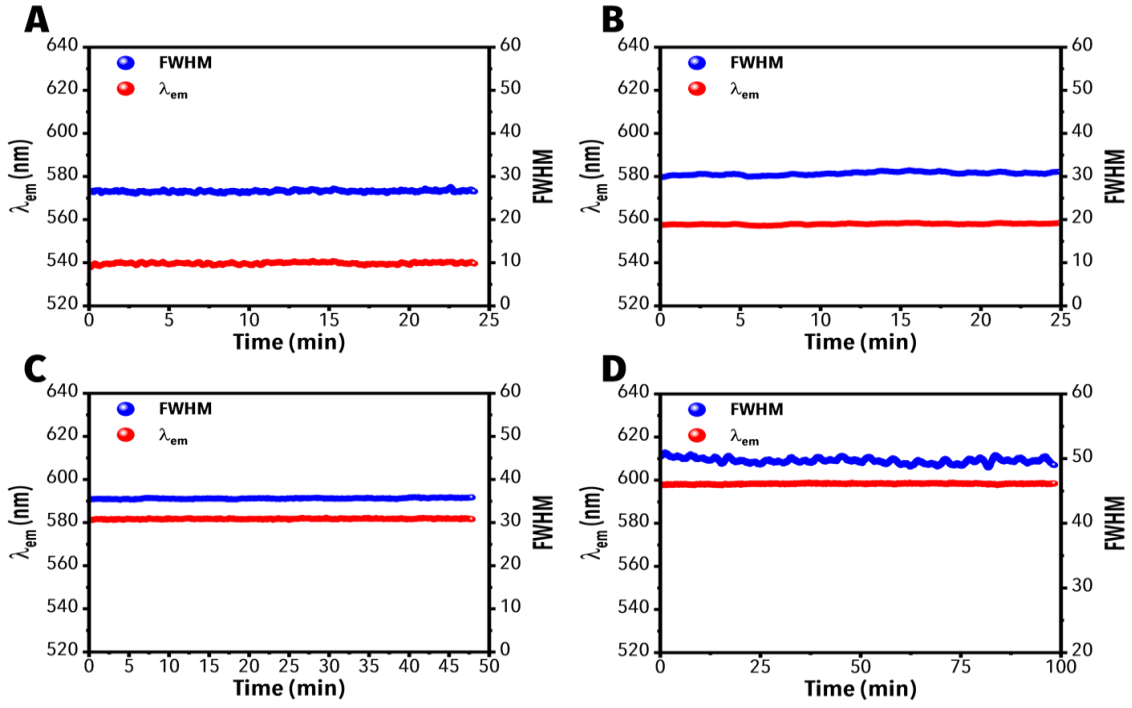

Figure A 7: Continuous Nanomanufacturing of CdSe Qd